The Canadian Mineralogist
Vol. 39, pp. 239-266 (2001)

OLIVINE–LIQUID RELATIONS OF LAVA ERUPTED BY KĪLAUEA VOLCANO FROM 1994 TO 1998: IMPLICATIONS FOR SHALLOW MAGMATIC PROCESSES ASSOCIATED WITH THE ONGOING EAST-RIFT-ZONE ERUPTION

CARL R. THORNBER[§]

U.S. Geological Survey, Hawaiian Volcano Observatory, Hawai'i Volcanoes National Park, Hawai'i 96718, U.S.A.

ABSTRACT

From 1994 through 1998, the eruption of Kīlauea, in Hawai'i, was dominated by steady-state effusion at Pu'u 'Ō'ō that was briefly disrupted by an eruption 4 km uprift at Nāpau Crater on January 30, 1997. In this paper, I describe the systematic relations of whole-rock, glass, olivine, and olivine-inclusion compositions of lava samples collected throughout this interval. This suite comprises vent samples and tube-contained flows collected at variable distances from the vent. The glass composition of tube lava varies systematically with distance and allows for the "vent-correction" of glass thermometry and olivine–liquid K_D as a function of tube-transport distance. Combined olivine–liquid data for vent samples and "vent-corrected" lava-tube samples are used to document pre-eruptive magmatic conditions. K_D values determined for matrix glasses and forsterite cores define three types of olivine phenocrysts: type A (in equilibrium with host glass), type B (Mg-rich relative to host glass) and type C (Mg-poor relative to host glass). All three types of olivine have a cognate association with melts that are present within the shallow magmatic plumbing system during this interval. During steady-state eruptive activity, the compositions of whole-rock, glass and most olivine phenocrysts (type A) all vary sympathetically over time and as influenced by changes of magmatic pressure within the summit-rift-zone plumbing system. Type-A olivine is interpreted as having grown during passage from the summit magma-chamber along the east-rift-zone conduit. Type-B olivine (high Fo) is consistent with equilibrium crystallization from bulk-rock compositions and is likely to have grown within the summit magma-chamber. Lower-temperature, fractionated lava was erupted during non-steady-state activity of the Nāpau Crater eruption. Type-A and type-B olivine–liquid relations indicate that this lava is a mixture of rift-stored and summit-derived magmas. Post-Nāpau lava (at Pu'u 'Ō'ō) gradually increases in temperature and MgO content, and contains type-C olivine with complex zoning, indicating magma hybridization associated with the flushing of rift-stored components through the eruption conduit.

Keywords: Hawai'i, Kīlauea, olivine tholeiite, rift zone, lava tube, glass thermometry.

SOMMAIRE

A partir de 1994 jusqu'à la fin de 1998, l'éruption de Kīlauea, île de Hawai'i, était dominée par une effusion stable et continue à Pu'u 'Ō'ō; celle-ci s'est vue interrompue brièvement par une éruption dans le cratère Nāpau, à 4 km de là en remontant le rift, le 30 janvier, 1997. C'est mon but dans cet article de décrire les relations systématiques de la composition des roches globales, du verre, de l'olivine et des inclusions piégées dans l'olivine des échantillons de lave prélevés au cours de cet intervalle. La suite inclut des échantillons pris des orifices et des coulées confinées aux tubes de lave, prélevés à distance variable de l'orifice. La composition du verre des laves prélevées dans les tubes varie systématiquement avec la distance et permet une correction des températures fondées sur la composition du verre et du rapport K_D pour le couple olivine–liquide en fonction de la distance parcourue. Une combinaison de données sur les couples olivine–liquide pour les échantillons des orifices et de données corrigées pour les échantillons pris dans les tubes sert à déterminer les conditions magmatiques pré-éruptives. Les valeurs de K_D déterminées sur le verre de la matrice et le coeur des phénocristaux d'olivine définissent trois types de phénocristaux: ceux de type A sont en équilibre avec le verre hôte, tandis que ceux de type B sont enrichis en Mg par rapport au verre, et ceux de type C sont appauvris en Mg, toujours par rapport au verre coexistant. Les trois types d'olivine partagent une association génétique avec les liquides en circulation durant cet intervalle dans le système de "plomberie" magmatique à faible profondeur. Au cours du stade éruptif soutenu, les compositions de roche globale, de verre et la plupart des phénocristaux d'olivine (de type A) varient toutes de façon uniforme avec le temps et selon les changements de pression magmatique au sein du système de rifts près du sommet. La croissance de l'olivine de type A aurait eu lieu lors du passage du magma de la chambre magmatique sommitale le long du conduit menant vers la zone de rift de l'est. L'olivine de type B (Fo élevé) aurait cristallisé à l'équilibre avec la composition globale des échantillons qui la renferment, et probablement à l'intérieur de la chambre magmatique sommitale. L'épanchement de laves de plus basse température, plus évoluées, a eu lieu lors de l'interruption des éruptions soutenues à partir du cratère de Nāpau. Les relations du

[§] *Current address*: U.S. Geological Survey, Cascades Volcano Observatory, 5400 MacArthur Boulevard, Vancouver, Washington 98661, U.S.A. *E-mail address*: cthornber@usgs.gov

couple olivine–liquide pour l'olivine de type A et de type B indiquent que ces laves sont des mélanges d'un liquide issu du système de rifts et d'un autre issu de la chambre sommitale. Les laves postérieures à l'effusion de Nāpau (signalées à Pu'u 'Ō'ō) augmentent graduellement en température et en teneur en MgO, et contiennent une olivine de type C, montrant une zonation complexe, indications d'une hybridisation de magmas associée au drainage du contenu des rifts et son écoulement dans le conduit éruptif principal.

(Traduit par la Rédaction)

Mots-clés: Hawai'i, Kīlauea, tholéiite à olivine, zone de rift, tube de lave, thermométrie fondée sur le verre.

Introduction

The basic configuration of the shallow magmatic plumbing system of Kīlauea Volcano, on the Island of Hawai'i, has been documented in numerous studies that correlate seismic and geodetic data with summit and rift-zone eruptive behavior (*e.g.*, Tilling & Dvorak 1993, and references therein). It is generally accepted that a continuously replenished shallow magmatic reservoir persists beneath Kīlauea's summit and that magma migrates laterally from the summit region through systems of shallow dikes propagated along radial rift-zones. The range of olivine tholeiite compositions erupted at the summit is principally restricted to that regulated by olivine-controlled fractionation occurring within the summit reservoir (MgO > 6.8 wt%: Wright & Fiske 1971). Rift zones serve both as magmatic conduits and as regions of magmatic storage where successive fractionation of olivine, plagioclase and clinopyroxene occurs during cooling . Thus, a broader range of lava chemistry is characteristic of rift-zone eruptions. Historically documented Kīlauea rift-zone eruptions of lava with chemically more evolved compositions are restricted to relatively short-lived eruptions with repose intervals of decadal duration (Wright & Fiske 1971, Wright 1971, Garcia *et al.* 1989, Helz & Wright 1992). During these brief eruptions, limited supplies of fractionated lava are interpreted to have been derived from shallow stagnant reservoirs that were variably diluted with hot and fresh olivine-saturated magmas.

In this paper, I describe the systematic relations of whole-rock, glass, olivine, and olivine-inclusion composition among 350 samples of rapidly quenched lava collected from September 1994 to December 1998. During this time, the ongoing 18-year-old east-rift-zone eruption was dominated by nearly continuous effusion of summit-derived olivine-controlled magma at Pu'u 'Ō'ō. This steady-state eruptive condition was briefly disrupted by an eruption of cooler, more fractionated lava 4 km uprift, at Nāpau Crater, on January 30, 1997. Samples of lava used for this investigation were obtained frequently throughout this eruptive interval, from both vent areas and from tube-contained flows. The temperature and glass composition of lava-tube samples varied systematically as a function of tube-transport distance and can be corrected to vent conditions. Vent and "vent-corrected" data provided herein constitutes the clearest possible indication of variations in pre-eruptive magmatic conditions over time. This unique suite of samples contains a petrological record of summit-rift zone conduit characteristics during intervals of both steady-state and non-steady-state eruptive activity. Comparative analysis of these eruptive products is pertinent to understanding how differentiated compositions are produced amidst sustained long-term rift-zone eruptions.

A "Roederesque" Approach

As particularly befitting this special collection of articles dedicated to Peter L. Roeder, a "Roederesque" approach of evaluating olivine–liquid systematics of 1994–1998 Kīlauea eruptive products is presented here. In hallmark experimental studies of olivine–liquid phase equilibria, Roeder & Emslie (1970) and Roeder (1974) described the basic systematics of the distribution of magnesium and ferrous iron between olivine and basaltic liquid. The equilibrium distribution coefficient, $K_D = (FeO/MgO)^{Ol} (MgO/FeO)^{Liq}$, was established as 0.30 (±0.03) and determined to persist essentially independently of variations in temperature and composition of basaltic liquids. This fundamental tenet of basalt petrology provides a simple and effective tool for discerning conditions of equilibration of well-quenched samples of molten olivine tholeiite erupted at Kīlauea Volcano. In this study, forsterite core compositions are used in conjunction with associated glass compositions to calculate an apparent K_D. K_D values derived in this manner allow an assessment of the degree of disequilibrium between phenocryst cores and coexisting melts. Both subtle and disparate deviations from equilibrium conditions of growth are identified and attributed to characteristics of pre- and post-eruptive eruptive magmatic history.

The samples reported on here provide temporal images of the dynamic eruptive plumbing system and, as such, are analogous to experimental run products from an enormously complicated laboratory apparatus (*i.e.*, Kīlauea Volcano). The challenge of studying them is to understand both the furnace and the run conditions. Petrological modeling of this unique time-series suite of eruptive products is constrained by real-time measurements of Kīlauea deformation during this eruptive interval. In this context, the observed olivine–liquid relations provide important clues to resolving shallow

magmatic processes that are inherent to long-term rift-zone eruptions of Hawaiian shield volcanoes.

Brief Overview of the East-Rift-Zone Eruption at Kīlauea

The flow field produced during 18 years of eruptive activity on the east rift zone of Kīlauea Volcano (through December, 1998) is shown in Figure 1. Published narratives describing the physical character of fifty-three discrete episodes of this eruption are as follows: Episode 1–47, from 1983 to 1986: Wolfe *et al.* (1988) and Heliker *et al.* (2000); Episode 48, from 1986 to 1992: Mattox *et al.* (1993), Garcia *et al.* (1996) and Kauahikaua *et al.* (1996); Episode 49, 1991: Mangan *et al.* (1995), and Episode 50–53, from 1992 to 1994: Heliker *et al.* (1998) and Kauahikana *et al.* (1998). Garcia *et al.* (1989) provided petrological evidence for mixing of rift-stored, clinopyroxene- and plagioclase-fractionated magma with hotter, olivine-controlled, summit-derived magma during the early phases of this eruption. The hybrid component of rift-stored magma had mostly cleared from the eruptive plumbing system by Episode 3 in April, 1983. During the high-fountain episodes of Pu‘u ‘Ō‘ō in 1985, the last remnants of differentiated rift-stored were completely flushed from the rift-zone conduit (Garcia *et al.* 1992). From 1985 and until the eruption revisited Nāpau Crater in January 1997, products of rift-zone eruption were restricted to olivine-saturated compositions fed by a nearly steady-state summit – rift-zone plumbing system (Garcia *et al.* 1996, Mangan *et al.* 1995, Heliker *et al.* 1998, and this paper).

By 1993 and through 1996, intra-crater pond activity at Pu‘u ‘Ō‘ō was accompanied by a single continuously active vent on the uprift flank of the Pu‘u ‘Ō‘ō cone (Episode 53, Heliker *et al.* 1998), and the eruption settled into a steady-state mode, with lava flow typically contained within a well-developed 10- to 11-km-long tube system from Pu‘u ‘Ō‘ō to the ocean. The 22-hour-long Nāpau Crater eruption on January 30 to 31, 1997 (Episode 54) immediately followed a well-documented,

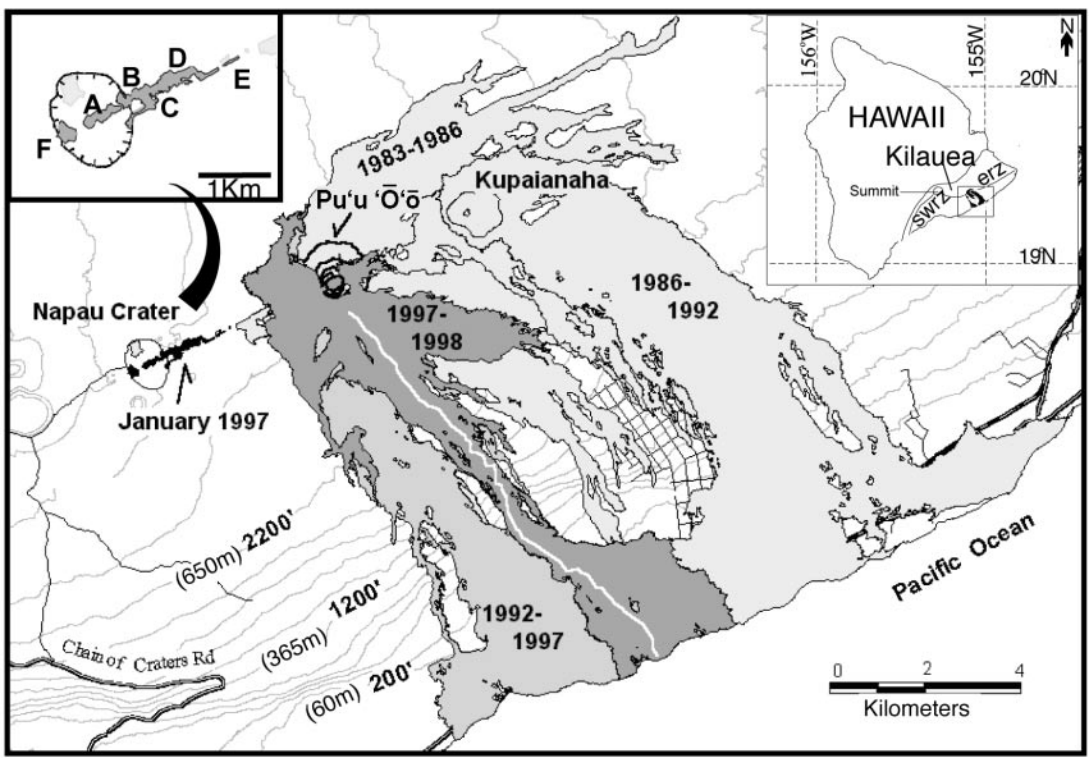

FIG. 1. Vent locations and lava flows of Kīlauea east rift zone eruptive activity, 1983–1998. Inset map in the upper right corner shows Hawai'i island and the location of this area along the east rift-zone (erz) of Kīlauea Volcano (swrz, southwest rift-zone). Episode 53 flow field (1992–1997) is shown in a medium dark shade. Darkest shaded area shows extent of Episode 55 flow field (1997–1998), with the main lava tube indicated as a white line. Fissure locations for the Episode 54, January 1997 Nāpau crater eruption are shown in the upper left inset. The sequence of Episode 54 eruption corresponds to the alphabetical order of fissure names (A, B, C, D, E and F).

shallow east-rift extensional event (Owen *et al.* 1997). This eruptive episode was sporadically fed from six northeasterly fissure vents along the rift (Fissures A through F, Fig. 1), extending from 2 to 4 km uprift of the Pu‘u ‘Ō‘ō vent area (Harris *et al.* 1998, Thornber *et al.* 1997). The current eruptive episode (Episode 55) began on February 24, 1997, when lava again appeared in the Pu‘u ‘Ō‘ō crater. Activity was limited to an active lava pond that steadily rose to the elevation of flank vents, which began to erupt on March 28, 1997. After three months of shield-building around sporadically active Pu‘u ‘Ō‘ō flank vents, a predominant outlet on the southwestern flank of the cone began to steadily feed a new easterly flow (see Fig. 1 in Cashman *et al.* 1999). The spatial and temporal evolution of the flow field from May through August 1997 is depicted in a time series of eruption maps in Harris & Thornber (1999). Through successive advancement of surface flows and tubes, lava reached the coast in mid-July; by August 1997, a relatively stable 11-km-long tube system was serving as a lava pipeline from the vent to the ocean. By mid-1997, steady-state eruptive conditions were re-established and have been maintained to the present time, with a mature tube system feeding lava from the vent to the ocean and with occasional tube overflows associated with brief and intermittent eruptive pauses. Between January and May 1998, steady-state eruptive activity was accompanied by occasional vent activity on the flank of Pu‘u ‘Ō‘ō.

The present study of olivine–liquid relations in the eruptive products of Kīlauea includes samples collected throughout intervals of steady-state eruptive activity of late Episode 53 and Episode 55 and the briefly intervening period of non-steady-state activity during Episode 54 and early Episode 55.

Petrological Sampling of Vent Tephra, Spatter and Tube-Contained Lava Flows

The goal of petrological sampling of this eruption is to monitor compositions at the vent through time. This is achieved through sampling of: 1) vent tephra and spatter, produced during sporadic intervals of low-level lava fountaining, 2) Pele’s tears and hair, frequently emitted from the active pond within Pu‘u ‘Ō‘ō, and 3) tube-contained lava flows, which are readily accessible at variable distances from the vent. Whereas tephra or tears are quickly air-quenched during deposition, it is most desirable to quench hot spatter or flow samples in water in order to minimize the growth of microlites that affect changes in glass composition.

Vent and tube samples during steady-state activity (late Episode 53 and late Episode 55)

During periods of steady-state eruptive activity, from September 1994 through January 1997 (Episode 53) and from July 1997 through December 1998 (Episode 55), lava samples were collected, to the extent possible, on a weekly basis both at the Pu‘u ‘Ō‘ō vent and from upper-elevation flow within the active tube system. In addition, samples of vent spatter were collected adjacent to sporadically active Pu‘u ‘Ō‘ō flank vents. Samples of sluggish and cooler tube flow that were collected during brief or intermittent pauses amidst otherwise steady-state activity are not included in this dataset, nor are any samples of distal surface flows.

Pele’s tears, hair, reticulite (tephra) and spatter from lava splashes within Pu‘u ‘Ō‘ō were collected at near-weekly intervals from wooden trays ($30 \times 60 \times 10$ cm) placed downwind of the lava pond on the rim of the active crater. There is an uncertainty of three to four days in the time of deposition of most of the air-quenched tephra collected from these “tear catchers”. Samples of tube-contained lava flows were taken at skylights created by roof collapses along the active tube system. These tube samples were routinely obtained at elevations above 600 m and over a distance ranging from ~1 to 6 km from the vent. The tube-flow sampling device consisted of a sledge-hammer head secured to the end of a 20-m length of 0.8 cm stainless-steel cable. In most cases, the cable-strung hammer head was tossed over a log positioned across the skylight in order to facilitate optimal positioning over the center of the flow and to avoid sample contamination by tube-roof material at the edge of the skylight. Using this technique, up to 0.5 kg of lava was retrieved from the tube flow and quickly and thoroughly quenched in water. All vent spatter samples were collected hot and quickly water-quenched in a manner similar to that described for vent sampling during non-steady-state eruptive activity.

Vent samples during non-steady-state activity

The first two samples from the January 30, 1997 Nāpau Crater eruption (Episode 54) were collected shortly after fountaining and flow had ceased at Fissure A (Fig. 1); their times of quenching are extrapolated on the basis of field relations and eye-witness reports of eruption. All other fissure-fountain spatter samples (Fissures B, D, E and F) reported here were still molten at the time of collection; these were retrieved by hand and water-quenched within seconds after their fall. Flow samples within 50 meters of vents were collected with geological picks from leading edges of fissure overflows or using cable-strung hammer heads tossed over levees into near-vent flow channels. Low-level fountain spatter and spatter-cone overflows or flow breaches from sporadic vents on the western and southwestern flanks of the Pu‘u ‘Ō‘ō cone, from May through July 1997 (early Episode 55), were sampled by similar methods.

Petrography of Samples Collected During Steady-State Activity

Aside from occasional microlites of plagioclase and clinopyroxene, olivine and chromian spinel are the only

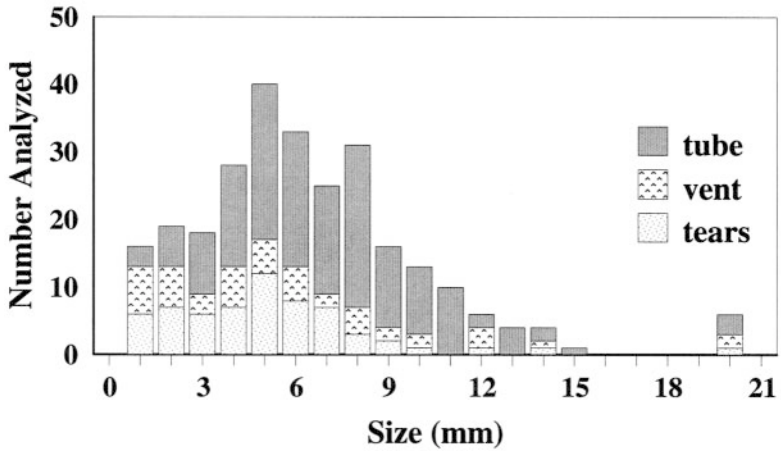

FIG. 2. Histogram showing the size distribution of analyzed phenocrysts of olivine in tube, vent and tear samples.

crystalline phases routinely present in Episode 53 and Episode 55 steady-state tear, vent and tube samples. These samples typically have 1 to 3 vol.% of olivine phenocrysts, up to 5 vol.% in a few Mg-rich samples. Olivine crystals can be as large as 2 mm, but are typically only 0.6 to 0.7 mm across, and there is no significant difference in size distribution among tear, vent or tube samples (Fig. 2). Electron-back-scatter images depicting the range of phenocryst textures observed in this sample suite are presented in Figures 3 and 4. Subhedral and euhedral microphenocrysts of chromian spinel are ubiquitously present in trace amounts, usually incorporated by olivine but occasionally present as isolated grains in glass. The olivine crystals in Pu'u 'Ō'ō tear samples are typically restricted to the more bulbous "droplet" portion of individual tears (Figs. 3A, B), and the modal abundance of olivine is usually around 1 vol.%. The slightly lower abundance of olivine compared to other vent or tube samples is most likely related to tear-formation mechanisms (Duffield *et al.* 1977, Shimozuru 1994), rather than to differences in character of the chemically homogeneous source of magma.

In tube samples, olivine occurs as free-floating crystals and in open-textured glomerocrystic aggregates (Fig. 3C). Schwindinger & Anderson (1989) attributed the latter texture in 1959 Kīlauea Iki lava to pre-eruptive synneusis. In this study, however, the synneusis of olivine crystals is attributed to flow dynamics either in the pre-eruptive conduit or in the lava tube.

Olivine phenocrysts in the entire suite of samples comprise an array of subequant to blocky and elongate crystals, and there is no clear correlation between crystal size and morphology. Subhedral phenocrysts (Figs. 3C, D) are typical and commonly coexist with less abundant, euhedral olivine (Figs. 3E, F). Both euhedral and subhedral skeletal and hopper-shaped crystals of olivine are present in many samples and display a range in size similar to that of subequant or elongate varieties. All morphological variants of olivine phenocrysts contain round to elongate glass inclusions, and inclusion-bearing olivine is present in nearly all samples analyzed. Numerous subhedral grains of olivine with abundant irregular inclusions are embayed in a fashion suggestive of rounded skeletal or hopper growth (Figs. 3G, H). Because there are no fine-scale cuspate textures at the interface between crystal embayments and glass, which would indicate significant chemical resorption due to crystal–melt disequilibria (Thornber & Huebner 1985), this embayed texture is interpreted to result from thermal erosion or abrasion at the crystal–liquid interface during near-equilibrium growth associated with dynamic transport within the rift-zone conduit. The subhedral to rounded shapes of most olivine grains in this suite of samples are suggestive of such pre-eruptive erosion or abrasion.

PETROGRAPHY OF SAMPLES COLLECTED DURING NON-STEADY-STATE ACTIVITY

Lava erupted during Episode 54 in Nāpau crater is variably choked with ~3 mm aggregates of plagioclase, clinopyroxene and olivine. These samples are ~20% to 50% crystalline and contain an assortment of rounded and angular phenocryst fragments that includes normally and reversely zoned pyroxene and plagioclase in addition to compositionally disparate olivine phenocrysts. Figure 4A shows a normally zoned and well-rounded olivine phenocryst with inclusions of relatively high-Mg glass in a matrix bearing skeletal and euhedral

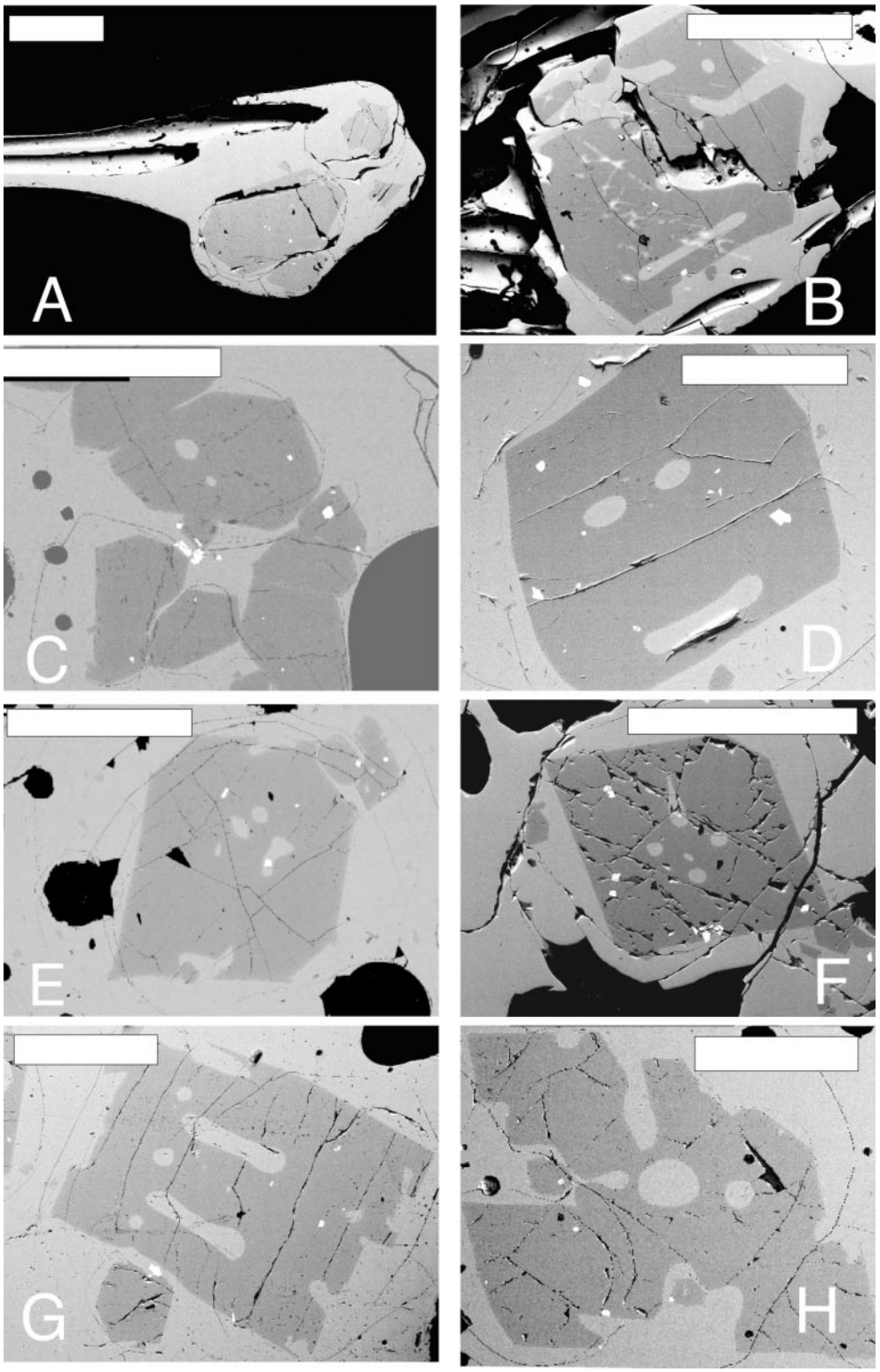
A
B
C
D
E
F
G
H

crystals of olivine. The fine-scale cuspate texture at the crystal–liquid interface of the rounded olivine phenocryst is evidence for partial resorption by the surrounding liquid. Other xenocryst-looking olivine phenocrysts display overgrowth of skeletal olivine on a finely cuspate and irregular core (Fig. 4B). Comparable examples of cuspate textures observed in hybrid magmas erupted in the Kīlauea 1959 summit eruption and in the 1955 lower east-rift eruption are interpreted as evidence for mixing of thermally and chemically disparate magmas (Thornber & Huebner 1985, Helz 1987, Helz & Wright 1992).

In material erupted early in 1997, from sporadic Pu'u 'Ō'ō flank vents, before steady-state conditions of eruption were re-established, variably reacted phenocrysts and olivine show complex zoning, distinct reaction-rims, and plagioclase inclusions (Figs. 4C–F). These textures are indicative of a complex temperature–composition history related to flushing of hybrid components through the shallow rift-zone conduit after the January 1997 magma-mixing episode. A small number of olivine grains, in samples of the subsequent Episode 55 steady-state eruption, display distinct normal or complex core–rim zonation patterns and are interpreted as erratic remnants from this flushing process (Figs. 4H, G).

Analytical Techniques

Concentrations of major elements were established in whole rocks by the U.S. Geological Survey (Denver), using X-ray fluorescence (XRF) techniques described by Taggart *et al.* (1987). Microbeam imagery and quantitative analyses used in this study were done at the USGS Denver Microbeam Facility using a JEOL 5900 scanning electron microscope (SEM) and a JEOL 8900 electron microprobe.

Electron-microprobe analyses of glass and minerals were done at 15 keV, 20 nA beam current and using a Phi–Rho–Z data-reduction routine. A 20-μm-diameter beam was used to minimize loss of alkalis during the analysis of glass. Data for major and minor elements were collected for 20-second peak-count intervals. A longer peak-count interval of 80 seconds was used for all sulfur determinations and produced reasonable results for concentrations above 100 ppm. Glass compositions used for all plots and calculations are the average result of 10 analyses per sample. One to three grains of olivine per sample were analyzed, along with glass inclusions, where present. Olivine crystals analyzed were selected by petrographic and SEM reconnaissance of each polished thin section. An average of two core compositions was obtained for one or more crystals of olivine of typical morphology and size in each sample analyzed. Rim compositions were determined for typical olivine grains in Episode 55 samples. In addition, core and rim compositions were established for any unusually large crystals or crystals with unusual and obvious zonation or reaction textures. Glass inclusions analyzed were usually greater than 80 μm in diameter and never less than 50 μm.

The precision of electron-microprobe results is estimated on the basis of counting statistics and reproducibility of standards that were repeatedly analyzed during each probe session. Most relevant to this study are the estimated errors in MgO and total FeO ($FeO_t = Fe_2O_3 + FeO$) concentrations used in glass-thermometry calculations [T°C = 20.1 * wt% MgO + 1014°C (Helz & Thornber 1987)] and in determining olivine–glass distribution coefficients [$K_D = (MgO/FeO)^{Ol} / (MgO/FeO)^{Liq}$ (Roeder 1974)]. Despite limitations in the absolute accuracy of the Helz–Thornber glass thermometer associated with an experimental uncertainty of 10°C, the relative temperatures estimated by this method are comparable within limits of analytical precision. MgO and FeO_t concentrations in glass and olivine standard samples are presented in Table 1. An average error of 1.4% (1σ) in determinations of MgO concentration in glass standards yields an average estimated precision of ±1.4°C in glass thermometry. An average of 1% (1σ) error in Mg:Fe ratio in olivine and glass standards translates to an estimated precision of 1% in calculated K_D

FIG. 3. Electron-back-scatter images of type-A olivine in eruption samples. In each photo, olivine appears dark gray amidst light gray host glasses. It contains light gray glass inclusions. Small crystals of chromian spinel appear as white flecks within and adjacent to most olivine grains. Black areas are vesicles. White bar-scale in each image is 500 μm. Each photo description includes sample type and number, morphology, olivine core composition (Fo), MgO-based glass temperature (MgO T°C) and olivine–glass K_D. "Vent-corrected" temperature and K_D are given for tube samples (MgO T°C* and K_D*; see text for explanation). A) Episode 53 Pu'u 'Ō'ō tear sample (KE53–1821T). Subhedral – blocky type-A olivine ($Fo_{80.6}$); MgO T°C = 1150°C; K_D = 0.299. B) Episode 55 Pu'u 'Ō'ō tear sample (KE53–1927T). Subhedral – embayed (hopper) type-A olivine ($Fo_{82.5}$); MgO T°C = 1164°C; K_D = 0.291. C) Episode 53 tube sample (KE53–1842F). Synneusis of subhedral crystals of type-A olivine ($Fo_{81.4}$); MgO T°C = 1149°C (MgO T°C* = 1154°C; K_D* = 0.295). D) Episode 53 tube sample (KE53–1834F). Synneusis of subhedral crystals of type-A olivine ($Fo_{80.9}$); MgO T°C = 1146°C (MgO T°C* = 1150°C; K_D* = 0.293). E) Early episode 55 tube sample (KE55–1911F). Euhedral – embayed type-A olivine ($Fo_{82.3}$); MgO T°C = 1148°C (MgO T°C* = 1151°C; K_D* = 0.267). F) Episode 55 tube sample (KE55–1997F). Euhedral type-A olivine ($Fo_{82.2}$); MgO T°C = 1157°C (MgO T°C* = 1162°C; K_D* = 0.292). G) Episode 53 tube sample (KE55–1964F). Blocky – embayed hopper type-A olivine ($Fo_{81.1}$); MgO T°C = 1150°C (MgO T°C* = 1154°C; K_D* = 0.291). H) Episode 53 tube sample (KE55–1722F). Subhedral – embayed, skeletal, hopper type-A olivine ($Fo_{82.2}$); MgO T°C = 1152°C (MgO T°C* = 1158°C; K_D* = 0.302).

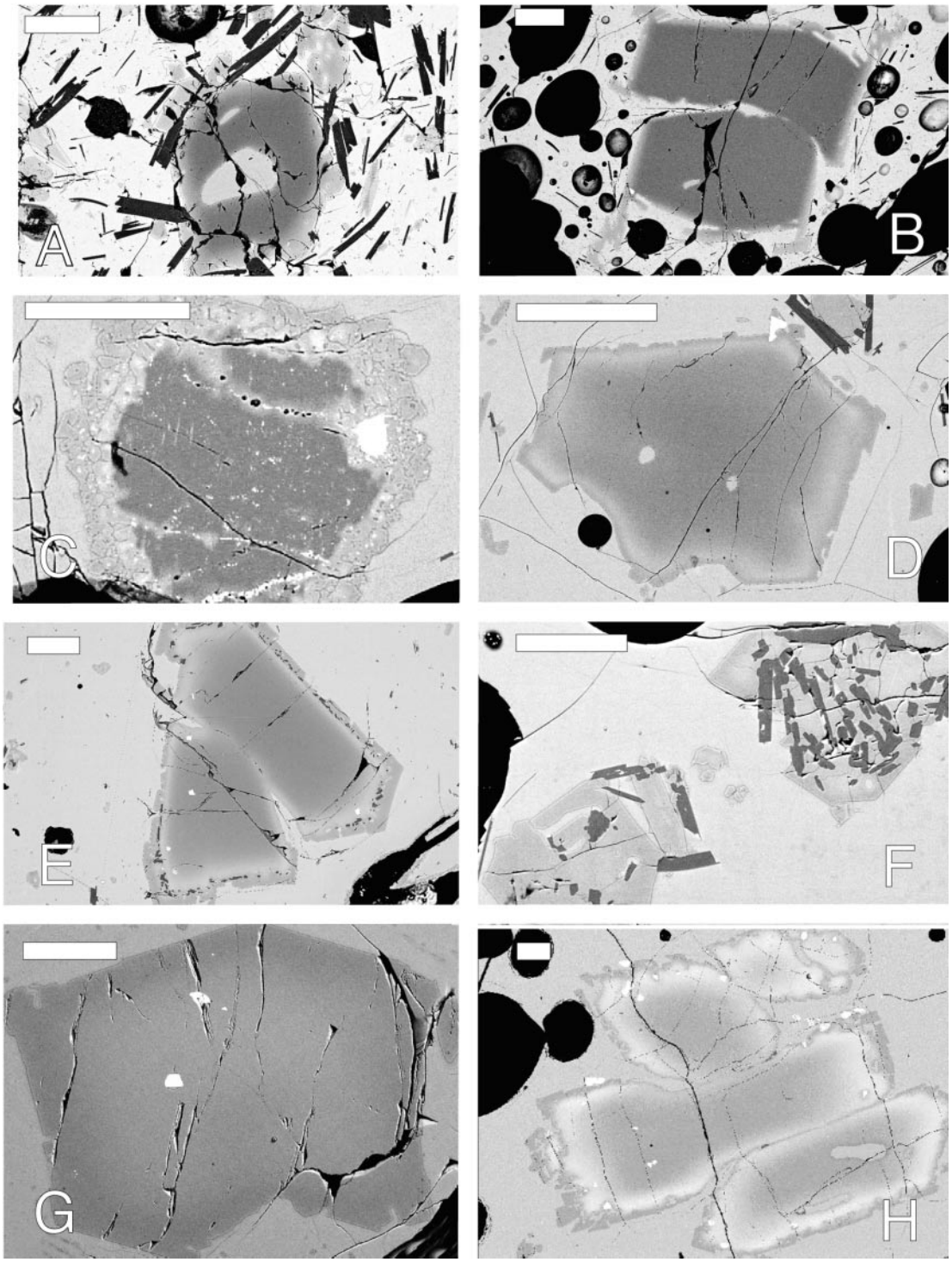
A
B
C
D
E
F
G
H

TABLE 1. REPRODUCIBILITY OF ELECTRON-MICROPROBE ANALYSES OF STANDARDS

	Glass				Olivine			
No. Anal.	VG-A99 369		USNM113716 72		SpringWater 58		Marjahlati 25	
	FeO_{total}	MgO	FeO_{total}	MgO	FeO_{total}	MgO	FeO_{total}	MgO
Average	13.15	5.03	9.04	8.08	16.8	44.18	11 5	48.6
Std. Dev.	0.14	0.08	0.1	0.11	0.22	0.4	0.08	0.53
Std. Value*	13.3	5.08	9.13	8.21	16.62	43.58	11 38	48.08

* Jarosewich *et al.* (1979) for the glass, Huebner & Woodruff (1985) for the olivine.

values (*e.g.*, $K_D = 0.300 \pm 0.003$). Both glass and olivine standards were found to be reproducible within the estimated precision in multiple electron-probe sessions over a four-year period, and no additional corrections to the data were made based upon standard variability over time (see Helz *et al.* 1995). The average standard deviation of wt% MgO per ten replicate analyses of glasses in all samples of this study is 1.4% (1σ), which demonstrates that unknown glasses are homogeneous within the estimated precision of analysis.

Ferrous iron (FeO) concentrations for whole-rock and glass were determined for five samples at Queen's University (P. Roeder and A. Grant, pers. commun., 1999), using the wet-chemical method described by Thornber *et al.* (1980). Results indicate an average whole-rock FeO/FeO_t value of 0.91 (σ = 0.01). Concentrations of FeO in the glass of each sample were calculated by subtracting the volume percent olivine with known FeO content from the whole-rock value. This approach yielded an average glass FeO/FeO_t value of 0.90 (σ = 0.01). On the basis of these measurements, a $FeO:FeO_t$ ratio of 0.9 is used to estimate FeO and Fe_2O_3 concentrations for all whole-rock and glass compositions. This value is the same as that used for Kīlauea lava in numerous other investigations (*e.g.*, Clague *et al.* 1995, Garcia *et al.* 1992, 1996).

Major-Element Composition of Whole Rocks and Matrix Glasses, and Glass Thermometry

Average major-element compositions for whole-rock (225 samples analyzed), and glass (2,940 analyses of 290 samples) are grouped according to eruptive interval and sample type (*i.e.*, tear, vent and tube) and presented in Appendix 1. The variations with time of whole-rock MgO (wt%) and MgO-based glass temperature (and corresponding wt% MgO in glass) in tube, tear and vent samples are presented in Figures 5A and 5B. The whole-rock MgO and the glass temperature vary sympathetically over time for the entire suite of tear, vent and tube samples. Late products of the Episode 53 eruption from September 1994 through January 1997 range from 7.1 to 9.6 wt% MgO and average 8.5 (σ = 0.2 wt%). Average MgO-based glass temperatures for this interval are 1152.7°C (σ = 3.2°) for Pu'u 'Ō'ō tears and 1150.0°C (σ = 2.9°) for tube samples (Appendix 1A). The short-lived January 1997 Nāpau fissures erupted relatively low-temperature basaltic liquid. Analyses of lava of Fissure A through E of Episode 54 reveal eruption temperatures of 1128 to 1138°C with an average whole-rock MgO of 6.4% (σ = 0.1) (Appendix 1B). Fissure F, the final and westernmost fissure, erupted lava at 1112° to 1124°C with an average whole-

FIG. 4. Electron-back-scatter images of olivine grains in non-steady-state eruption samples. General description of images is the same as for Figure 3; crystals of plagioclase are very dark gray, and crystals of augite are lighter gray compared to olivine. White bar-scale each image is 100 μm. A) Episode 54 Fissure F vent sample (KE54–1864F). Round type-B olivine (center) ($Fo_{84.5}$ core and $Fo_{77.7}$ rim) with cuspate margins and glass inclusion (MgO T°C incl. = 1130 °C). Plagioclase, augite and type-A olivine ($Fo_{72.2}$) in glass matrix (MgO T°C = 1116 °C); type-B olivine – host glass $K_D = 0.145$; type-A olivine – host glass $K_D = 0.306$. B) Episode 54 Fissure F vent sample (KE54–1867F). Round type-B olivine (center) ($Fo_{84.0}$ cores and $Fo_{78.9}$ rim) with cuspate margins overgrown by skeletal type-A olivine (Fo_{76}) extending into matrix glass. Plagioclase, augite and olivine in glass matrix (MgO T°C = 1123 °C); type-B olivine – host glass $K_D = 0.169$; type-A overgrowth – host glass $K_D = 0.279$. C) Episode 55 tube sample (KE55–1911F). Resorbed and reacted type-B olivine with type-C olivine (plus glass) overgrowth ($Fo_{85.1}$ core and $Fo_{76.4}$ overgrowth) with reacted chromian spinel inclusion. (MgO T°C* = 1151°C; type-B olivine – host glass $K_D^* = 0.218$; type-C overgrowth – host glass $K_D^* = 0.377$). D) Episode 55 tube sample (KE55–1911F). Complexly zoned olivine with type-B core ($Fo_{84.2}$), type-C inner rim ($Fo_{78.5}$) and type-A skeletal overgrowth ($Fo_{81.2}$). (MgO T°C* = 1151°C; type-B olivine – host glass $K_D^* = 0.234$; type-C inner rim – host glass $K_D^* = 0.318$; type-A overgrowth – host glass $K_D^* = 0.293$). Plagioclase and type-A olivine (Fo_{80}) in glass matrix (matrix – host glass $K_D = 0.318$). E) Episode 55 vent sample (KE55–1909F). Complexly zoned olivine with type-B core ($Fo_{83.8}$), type-C inner rim ($Fo_{77.7}$) with plagioclase intergrowth, and type-A skeletal overgrowth ($Fo_{80.1}$). (MgO T°C = 1151°C; type-B olivine – host glass $K_D^* = 0.238$; type-C inner rim – host glass $K_D^* = 0.365$; type-A overgrowth – host glass $K_D^* = 0.310$). F) Episode 55 vent sample (KE55–1871F). Reversely zoned type-C olivine with plagioclase inclusions (MgO T°C* = 1149°C). G) Episode 55 tube sample (KE55–1935F). Reversely zoned olivine with type-C core ($Fo_{77.5}$) and type-A rim ($Fo_{81.3}$). (MgO T°C* = 1158°C; type-C olivine – host glass $K_D^* = 0.372$; type-A rim – host glass $K_D^* = 0.287$). H) Episode 55 tube sample (KE55–2027F). Complexly zoned olivine with type-A core ($Fo_{82.8}$), type-C inner rim ($Fo_{70.6}$) and type-A skeletal overgrowth ($Fo_{82.7}$). (MgO T°C* = 1158°C; type-A olivine – host glass $K_D^* = 0.282$; type-C inner rim – host glass $K_D^* = 0.563$).

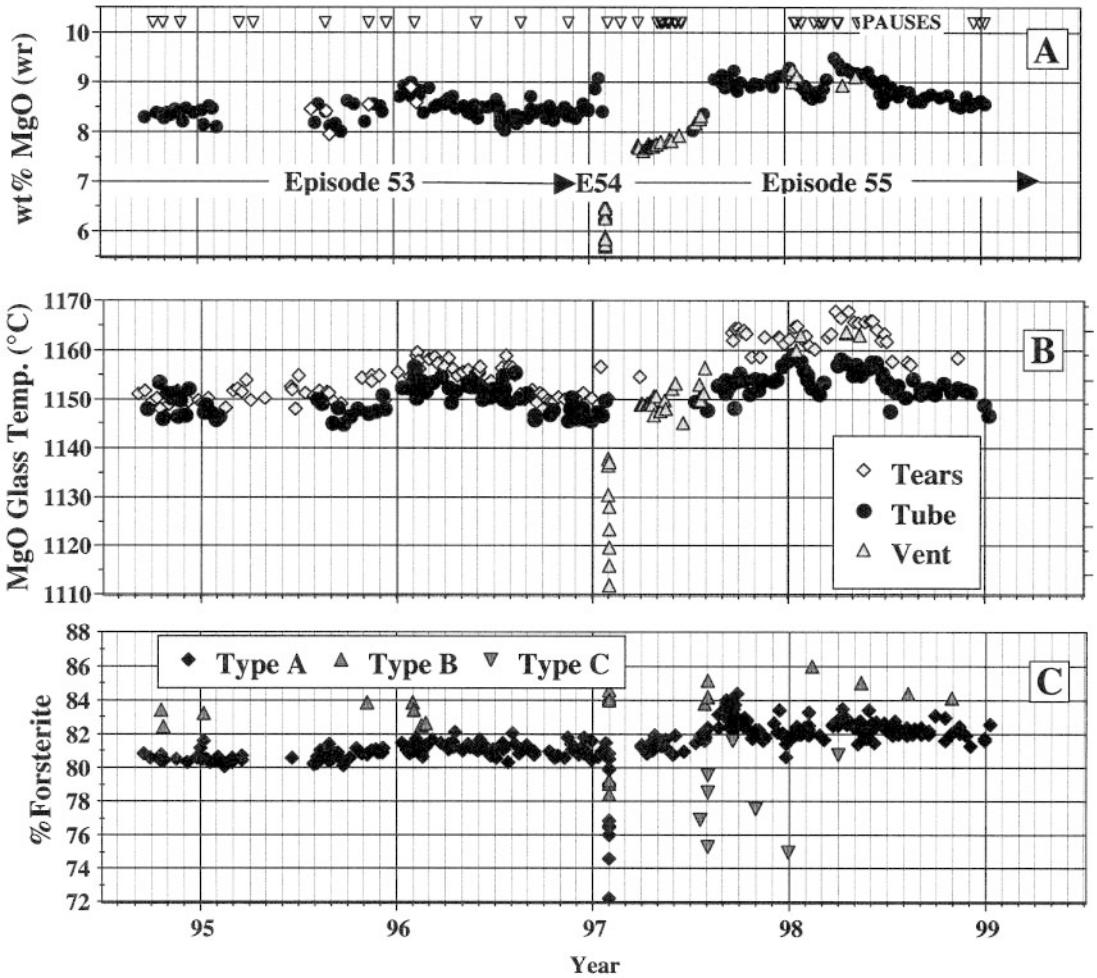

FIG. 5. Time-series plot of A) Whole-rock wt% MgO, B) MgO-based glass thermometry (and wt% MgO), and C) % Forsterite in olivine, for samples collected from September, 1994 through December, 1998. Episode 53, 54 and 55 durations are indicated in A, which also shows the timing of brief eruptive pauses (down-pointing triangles plotted along the top of the diagram). In A and B, tear samples are shown as unfilled diamonds, vent samples are shaded up-pointing triangles, and tube samples are black circles. In C, type-A olivine is shown as black diamonds, type-B olivine is represented by shaded up-pointing triangles, and type-C olivine, by shaded down-pointing triangles.

rock MgO of 5.8% (σ = 0.1).Early during Episode 55, before steady-state eruptive conditions were re-established, the MgO content of lava issued from sporadic Pu‘u ‘O‘ō flank vents increased steadily with time from 7.7 to 8.3% MgO, and eruption temperatures increased from 1145° to 1156°C (Appendix 1C). By August 1997 and through December 1998, products of Episode 55 steady-state eruptive activity have had the highest temperature and most Mg-rich compositions in the entire history of this eruption (compare Helz & Hearn 1998). MgO-based glass temperatures of late Episode 55 Pu‘u ‘O‘ō tear and vent samples range from 1157° to 1168°C, and average 1163°C (σ = 2.7°C). Episode 55 tube samples have temperatures that range from 1147° to 1159°C , and average 1154°C (σ = 2.7°). Whole-rock MgO of tube and vent samples during this interval ranges from 8.5 to 9.5%, with an average value of 8.9 (σ = 0.2%) (Appendix 1D).

Figure 6 shows the whole-rock compositions of the late 1994 through 1998 suite of samples on a plot of CaO *versus* MgO concentrations. The compositional variation for these eruption products follows typical fractionation trends of Kīlauean lavas (*e.g.*, Wright 1971, Wright & Fiske 1971, Helz & Wright 1992). Late Episode 53 and Episode 55 Ca–Mg variations are tightly constrained by olivine control to ~7.5 wt% MgO. Be-

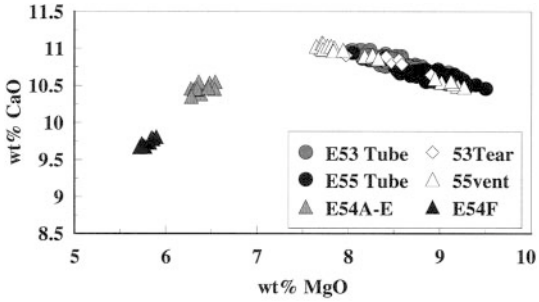

FIG. 6. Whole-rock wt% CaO variation with wt% MgO for September, 1994 through December, 1998 samples. Symbols are as shown in the legend for Episode 53, 55 tube, tear and vent samples and Episode 54 Fissures A–E and Fissure F vent samples. Episode 53 and Episode 55 samples define an olivine-control trend, the low-Mg end of which is defined by early Episode 55 non-steady-state vent samples.

low this value, coprecipitation of augite and plagioclase cause Ca to decrease linearly with Mg. There are two compositions of chemically distinct evolved magma erupted during Episode 54 at Fissures A–E and Fissure F, with MgO average contents of 6.4 and 5.8%, respectively. Lava from Fissures A–E is interpreted as a mixture of hotter, rift-conduit magma with cooler and fractionated magma stored within the rift-zone and erupted at Fissure F.

Among concurrent steady-state tube, tear and vent samples, tube samples have consistently lower MgO-based glass temperatures (Fig. 5B), reflecting minor overgrowth of olivine phenocrysts associated with cooling during transport. CaO *versus* MgO variation in tear glasses (Fig. 7A) defines an olivine-control trend consistent with that of whole-rock data (primarily from tube samples), but Ca content of tube and vent glasses is more scattered (Fig. 7B). Since the eruption temperature reflected by tear samples is close to the temperature at which augite and plagioclase begin to crystallize (*i.e.*, between 1150 and 1160°C: Helz & Thornber 1987, Thompson & Tilley 1969), it follows that the minor disparity between compositional trends of whole rocks and glass of tube and vent samples is related to a small amount of microlite crystallization associated with syn- and post-eruptive cooling. This suggestion is borne out by the observation of trace amounts of plagioclase and augite microlites in many tube and vent samples. Microlites in tube samples develop because of minor cooling during downtube transport. Many spatter samples collected during sporadic low-level fountaining at vents are variably microlite-rich because air-cooled lava is recycled within the vent during cyclic pulses of fountaining activity.

THE COMPOSITIONAL RANGE OF OLIVINE

Average results of 542 analyses of 357 olivine cores in 258 samples are presented in Appendix 1 and grouped according to eruptive interval, sample type (*i.e.*, tear, vent and tube) and phenocryst type (as described below). The variation of measured forsterite (Fo) content of olivine cores in individual tear, tube and vent samples over time is presented in Figure 5C for comparison with

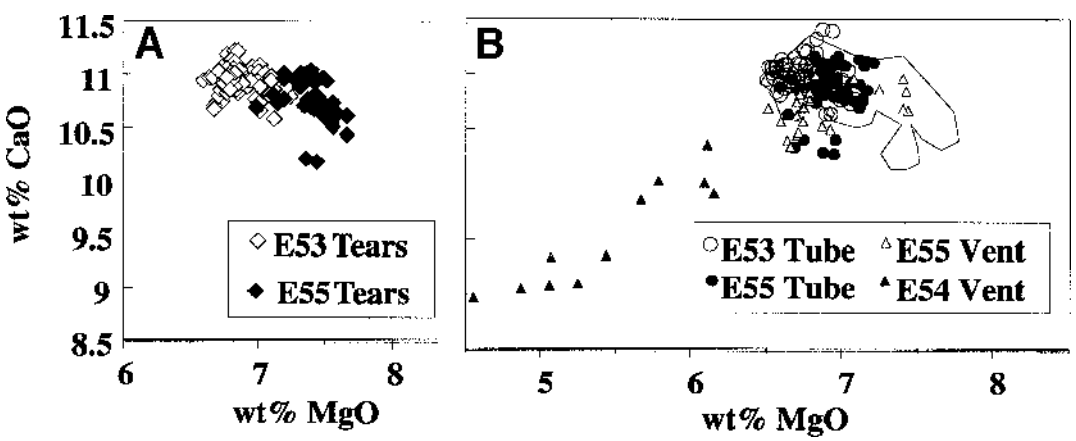

FIG. 7. Variation with MgO of CaO as a function of MgO (wt%) in glass for September, 1994 through December, 1998 samples. A) Compositions of steady-state Episode 53 (unfilled diamonds) and Episode 55 tear samples (filled diamonds). B) Compositions of steady-state tube samples for Episode 53 (unfilled circles) and Episode 55 (black circles), and non-steady-state vent samples during Episode 54 (shaded up-pointing triangles) and Episode 55 (unfilled up-pointing triangles). The field of tear samples from A is shown for comparison.

variations in both glass and whole-rock composition (Figs. 5A, B). There is no correlation between olivine composition and sample type. Of the olivine grains analyzed, 88% have core compositions that vary sympathetically with the temporal variation of whole-rock composition and glass temperatures, and 12% do not conform with this trend. Comparison of temporal trends for host glass and phenocryst cores provides a first-order basis for distinguishing three types of phenocrysts (labeled A, B and C). Core compositions of type-A olivine vary consistently with host-glass compositions over time. Relative to type-A olivine, cores in concurrent type-B olivine have high Fo contents, and cores in type-C olivine have low Fo contents. The number of olivine grains analyzed per sample is insufficient for quantitative evaluation of the frequency and distribution of the different types of olivine. Nonetheless, care was taken to analyze both representative and unusual phenocrysts in a large number of samples in order to minimize bias in the population of olivine grains analyzed. A summary of the general physical and chemical characteristics of these types of olivine in each eruptive episode is presented in Table 2.

Core compositions in type-A olivine range from Fo_{80} to Fo_{82} in Episode 53 (Appendix 1A), from Fo_{81} to Fo_{84} in Episode 55 (Appendix 1C and D), and from Fo_{75} to Fo_{80} in variably fractionated Episode 54 lavas (Appendix 1C). Core compositions in type-B olivine range from Fo_{83} to Fo_{85} in Episodes 53 and 55 samples, and from Fo_{75} to Fo_{84} in Episode 54. Type-C olivine is observed only in Episode 55, and ranges in core composition from Fo_{75} to Fo_{80}. A more detailed evaluation of the compatible and incompatible compositional relationships of olivine and host lava, which supports the distinction among olivine types as outlined here, is discussed later in terms of calculated olivine–liquid distribution coefficients for vent and tube samples.

In steady-state eruption samples, the morphology and size range of type-B olivine are generally indistinguishable from those of type A. Figure 8 is a time-series plot of compositions of phenocryst cores and outermost rims of type-A, -B and -C olivine in Episode 55 samples. Grains of type-A olivine are either unzoned or have a slightly iron-enriched outer rim (<50 μm) compared to more extensive normal zoning of type-B (>50 μm) and reversed zonation of type-C phenocrysts. In evolved melts of Episode 54, grains of type-A olivine occur within glomerophyric aggregates of augite and plagioclase or as free-floating euhedral to skeletal crystals. Type-B olivine displays cuspate, resorbed outer edges (Figs. 4A, B). Some type-B olivine phenocrysts in early Episode 55 samples have complex core–rim

TABLE 2. GENERAL CHARACTERISTICS OF OLIVINE PHENOCRYSTS IN PRODUCTS OF 1994–1998 ERUPTIONS

	Type-A Olivine			Type-B Olivine			Type-C Olivine
	Episode 53	Episode 54	Episode 55	Episode 53	Episode 54	Episode 55	Episode 55
Core composition (range, %Fo)	Fo 80 – 82	Fo 75 – 80	Fo 81 – 84	Fo 83 – 84	Fo 78 – 84	Fo 83 – 85	Fo 75 – 82
Morphology	Subhedral, euhedral, hopper crystals; free-floating crystals, loose aggregates	Glomerophyrically intergrown with Pl, Cpx; free-floating euhedral - skeletal crystals	Subhedral, euhedral, skeletal and hopper crystals; free-floating crystals, loose aggregates	Subhedral to euhedral free-floating crystals	Round with cuspate outer margins; angular fragments	Round to subhedral and euhedral; occasional skeletal rims; free-floating crystals	Round to subhedral cores and subhedral to euhedral or skeletal rims; free-floating crystals, some with Pl inclusions
Core-to-rim Zonation	Unzoned or slight normal zoning (<50 μm rim)	Unzoned	Unzoned or slight normal zoning (<50 μm rim)	Normal zoning (>50 μm rim)	Normal zoning, variable rim development	Normal zoning, >50 μm rim; some complex zoning	Reverse or complex zonation (or both)
Olivine core /host melt compatibility*	Compatible $K_D \approx 0.30$	Compatible $K_D \approx 0.30$	Compatible $K_D \approx 0.30$	Incompatible $K_D < 0.30$	Incompatible $K_D < 0.30$	Incompatible $K_D < 0.30$	Incompatible $K_D > 0.30$

* (Ol–L K_D). Symbols: Cpx clinopyroxene, L liquid, Ol olivine, Pl plagioclase.

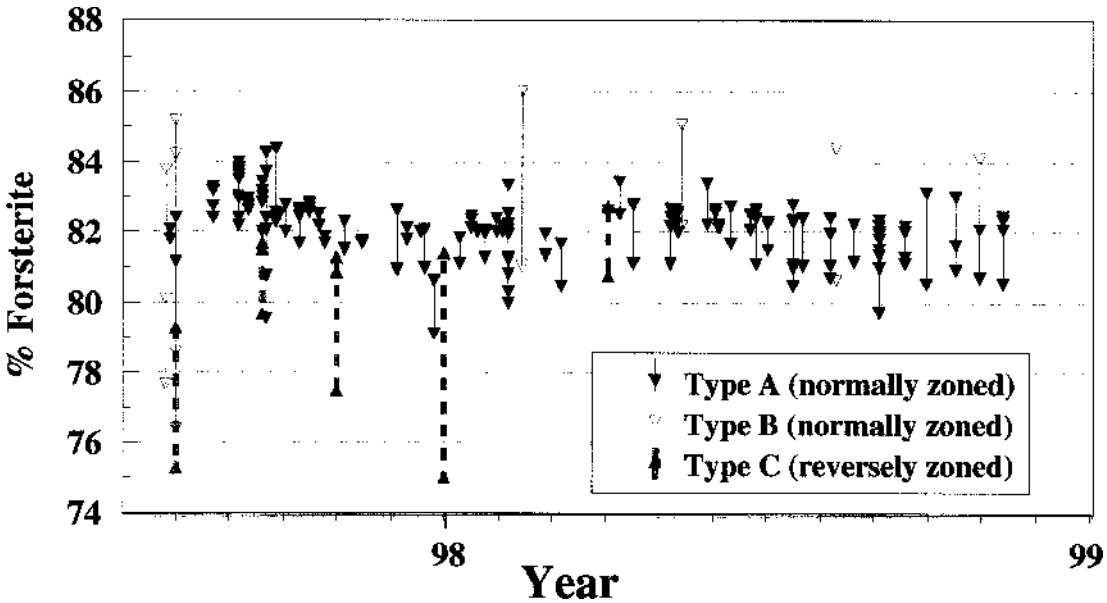

FIG. 8. Time-series plot of percentage Fo in olivine cores and outermost rims for Episode 55 samples. Tie-lines are drawn between individual core–rim pairs. Type-A olivine (black down-pointing triangles) displays a small range of normal zoning; type-B olivine (unfilled down-pointing triangles) shows more extensive normal zoning, and type-C olivine (shaded up-pointing triangles) has reversely and complexly zoned patterns.

zonation or reaction coronas (Figs. 4C–E), reflecting a more complicated magmatic history. Type-C olivine is distinguishable by complex and reversed patterns of zoning, or the presence of plagioclase inclusions (Figs. 4F–H).

GLASS INCLUSIONS IN OLIVINE

Average compositions of glass inclusions in 162 grains of olivine from 144 samples are presented in Appendix 1. Electron-back-scatter images of typical inclusion-bearing olivine are shown in Figure 3. Aside from occasional chromian spinel, around which some inclusions form, these domains of glass are devoid of crystalline phases. The MgO content of glass inclusions in this suite ranges from 5.3 to 7.6 wt%, with a MgO-based glass-temperature range of 1120° to 1167°C. Inclusion compositions and glass temperatures correlate reasonably well with those of host glasses in most tear samples, but are poorly correlated with host glasses in most Episode 53 and 55, tube and vent samples (Fig. 9). The Mg contents of glass inclusions in type-A olivine from tube and vent samples are generally low relative to those for host glasses, and are slightly lower but broadly consistent with host glasses in tear samples. In Figure 10, measured core compositions of olivine (types A and B) are compared with those calculated using compositions of associated glass inclusions (using K_D = 0.300; Roeder & Emslie 1970). Average values of %Fo calculated from included glasses for each sample type and eruptive interval are presented in Appendix 1. Calculated Fo values are slightly lower than, but consistent

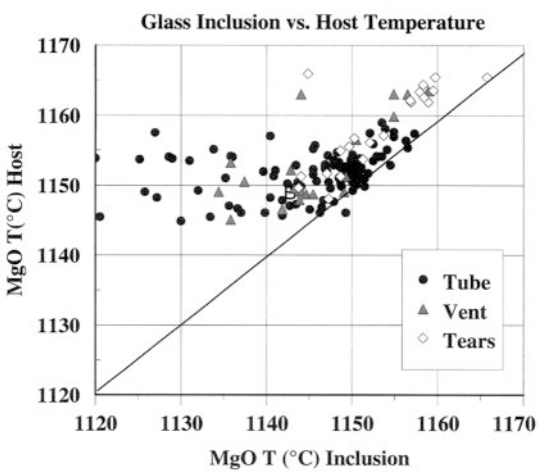

FIG. 9. MgO-based glass thermometry (°C) for coexisting glass inclusions in olivine and host glasses in tube, tear and vent samples (symbols as shown in key).

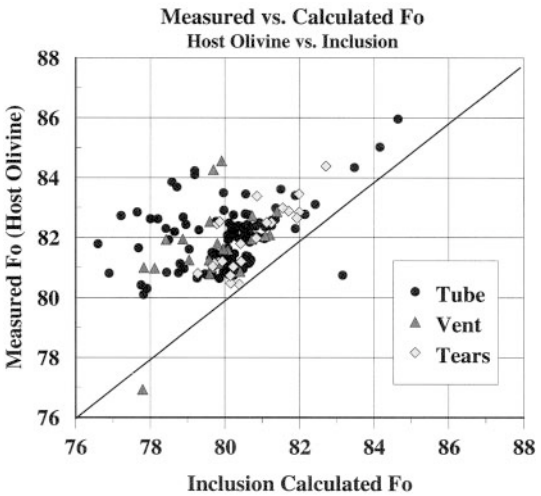

FIG. 10. Measured % Fo in olivine cores *versus* that calculated from coexisting inclusions in olivine (assuming K_D = 0.30) in tube, tear and vent samples. Symbols are the same as in Figure 9.

with, measured compositions of olivine cores in tear samples, although Fo depletion of inclusions is erratic and much greater in other samples. Schwindinger & Anderson (1989) and Clague *et al.* (1995) attributed the chemical disparity of glass inclusions to post-entrapment crystallization of olivine along inclusion walls. However, detailed image-analysis of inclusion walls was not conducted in this or other studies, and physical evidence for that process is lacking. The comparison of olivine-inclusion and host-glass composition with sample type indicates that disparities are associated with varying degrees of pre- and post-eruptive cooling. The slight but systematic offset of inclusion compositions in tear samples demonstrates that minor post-entrapment crystallization is a consistent feature in juvenile vent samples and is likely to have occurred prior to eruption. The erratic compositional variation of inclusions in samples of tube flow or vent spatter suggests that cooling during transport within tubes or during sporadic fountaining of spatter cones may result in rapid growth of olivine along melt-inclusion walls. Such unpredictable variations in compositions of inclusions in olivine severely limit their usefulness as a proxy for compositions of juvenile magma, particularly in tube-fed lava flows.

Ca–Mg relations of included glasses in all sample types are compared to those of bulk glasses in tear samples and to other published data on olivine inclusions at Kīlauea in Figure 11. The inverse variation of Ca and Mg of this suite of inclusions defines an approximate olivine-control trend that is collinear with tear data, but extends to much lower Ca contents owing to the

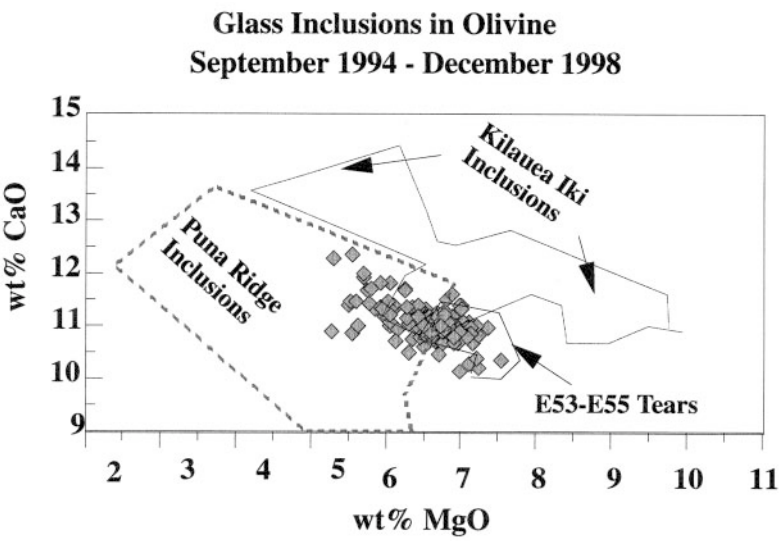

FIG. 11. Variation of CaO with MgO wt% in glass inclusions in olivine of all samples compared to other Kīlauea olivine glass-inclusion data and Episode 53–55 tear glasses. The field of glass inclusions of Kīlauea Iki samples (dark line) is from Schwindinger & Anderson (1989). Data of Puna Ridge glass inclusions (dashed line) is from Clague *et al.* (1995), and the field of Pu'u 'O'ō tear glasses (heavy dark line) is from Figure 7A.

post-entrapment crystallization of olivine along inclusion walls. Despite this artifact of olivine depletion, the overall chemical variation of inclusions in olivine demonstrates the compositional compatibility among all inclusion-bearing olivine grains in this suite of lava samples. Compared to the range of olivine inclusions in Kīlauea Iki tephra (Schwindinger & Anderson 1989), the data gathered in this study indicate that inclusion-bearing olivine in erupted samples crystallized from an initial magma that was more differentiated than the Mg-rich Kīlauea Iki magma. In contrast, the compositional array of microlite-free inclusions from Puna Ridge (Clague *et al.* 1995) reflects host-olivine crystallization from a wide range of variably fractionated magmas erupted along Kīlauea's east rift-zone.

The average concentration of sulfur in glass inclusions is ~500 ppm. Sulfur concentration ranges from less than 100 ppm to 1300 ppm (Appendix 1). Sulfur values in glass inclusions are distinctly higher than those of host glasses, which usually contain less than 100 ppm and attain 450 ppm. No correlations exist between sulfur concentration in inclusions or host glasses with sample type, glass temperature or olivine composition. Inclusions in type-B olivine have higher average levels of sulfur than those in type-A olivine, but the range of sulfur concentration in both types is similar. An overall higher concentration of sulfur in glass inclusions relative to host glasses suggests that, in most cases, the olivine formed in a relatively sulfur-rich or undegassed magma.

Glass Thermometry and Olivine–Liquid Systematics of Tube-Contained Lava Flows

Significant post-eruptive changes in temperature, crystallinity, and bulk composition occur during transport and emplacement of lava flows on the surface (*e.g.*, Cashman *et al.* 1999, Sharma *et al.* 1999). As a result, compositional data on distal lava flows cannot be used to resolve subtle changes in pre-eruptive magmatic conditions. In contrast, lava transported within thermally efficient tubes is subjected to only minor cooling and thus retains a better record of pre-eruptive attributes. Linear decreases in lava temperature with distance of down-tube transport have been documented at ~1°C/km during the 1971 Mauna Ulu eruption (Swanson 1973) and ~0.6°C/km during Episode 48 of the current eruption (Cashman *et al.* 1994, Helz *et al.* 1991, 1993). These rates of cooling are compatible with those implied by theoretical analysis of the thermal efficiency of lava tubes (Sakimoto *et al.* 1997, Keszthelyi 1995). Compositional changes associated with down-tube transport and cooling of lava can be corrected to vent conditions, thus allowing the use of lava-tube samples for interpretation of subtle pre-eruptive magmatic variations.

Upper-elevation tube samples used in this investigation were taken at distances of up to 5.9 km along the tube system (Appendix 1). As shown in Figure 5B, the Mg-based glass temperatures of these tube samples are lower than those for Pu'u 'O'ō tear samples collected over the same intervals of steady-state activity. To quantify changes in glass composition associated with transport distance within the tube and thus establish a means for correcting the glass compositions of tube samples to vent conditions, same-day down-tube sampling experiments were conducted during Episode 53 and Episode 55 steady-state activity.

Olivine–glass compositional variations for five same-day down-tube suites of samples are presented in Figure 12. Each of these sample suites includes multiple tube samples collected on the same day at distances ranging from 3.6 to 9.4 km along the tube system. In addition, each dataset includes Pu'u 'O'ō tear samples formed within a few days of each down-tube sample series. In four of the five sample suites (5/09/96, 5/29/96, 1/09/97 and 9/03/98), glass temperature decreases with distance of transport from the vent, at a rate of 0.5° – 1.3°C/km (Fig. series 12A; average $R^2 = 0.94$). In these four suites of samples, the up-tube projection of temperature corresponds closely to glass temperatures of tears at the Pu'u 'O'ō vent (all below 1160°C). These results are consistent with down-tube rates of cooling estimated from previous studies. However, in the 09/05/97 same-day suite, the glass temperature of Pu'u 'O'ō tears (1164°C) is 8°C higher than that indicated by a linear projection of down-tube temperatures, which decrease at 0.9°C/km. The rapid early cooling experienced by this lava may reflect small amounts of latent heat contributed by early crystallization of olivine (at T>1160°C), compared to that of two- or three-phase crystallization at lower temperatures during tube transport. As shown by Helz *et al.* (1993), the thermal efficiency of lava transport within tubes is significantly enhanced by latent heat evolved during crystallization of trace amounts of clinopyroxene and plagioclase microlites.

Compositional relations of olivine–glass pairs in same-day, down-tube suites are evaluated in order to establish a correction to vent conditions of the measured distribution-coefficient for FeO and MgO between olivine cores and host glasses in tube samples. Plots of measured Fo content of type-A olivine cores *versus* Fo calculated from host glass compositions (assuming an equilibrium $K_D = 0.300$: Roeder & Emslie 1970) for same-day down-tube sample suites demonstrate that olivine retains core-composition integrity during down-tube transport, whereas surrounding melts become progressively more magnesium-depleted (Fig. series 12B). A nominal average cooling-rate of 0.9°C/km for all same-day down-tube suites is correlated with an average change in the measured K_D value between olivine cores and host glasses of 0.002/km. These average correction-factors are applied to all upper-elevation tube samples, providing a "vent correction" for measured glass temperature and olivine–liquid K_D that is depen-

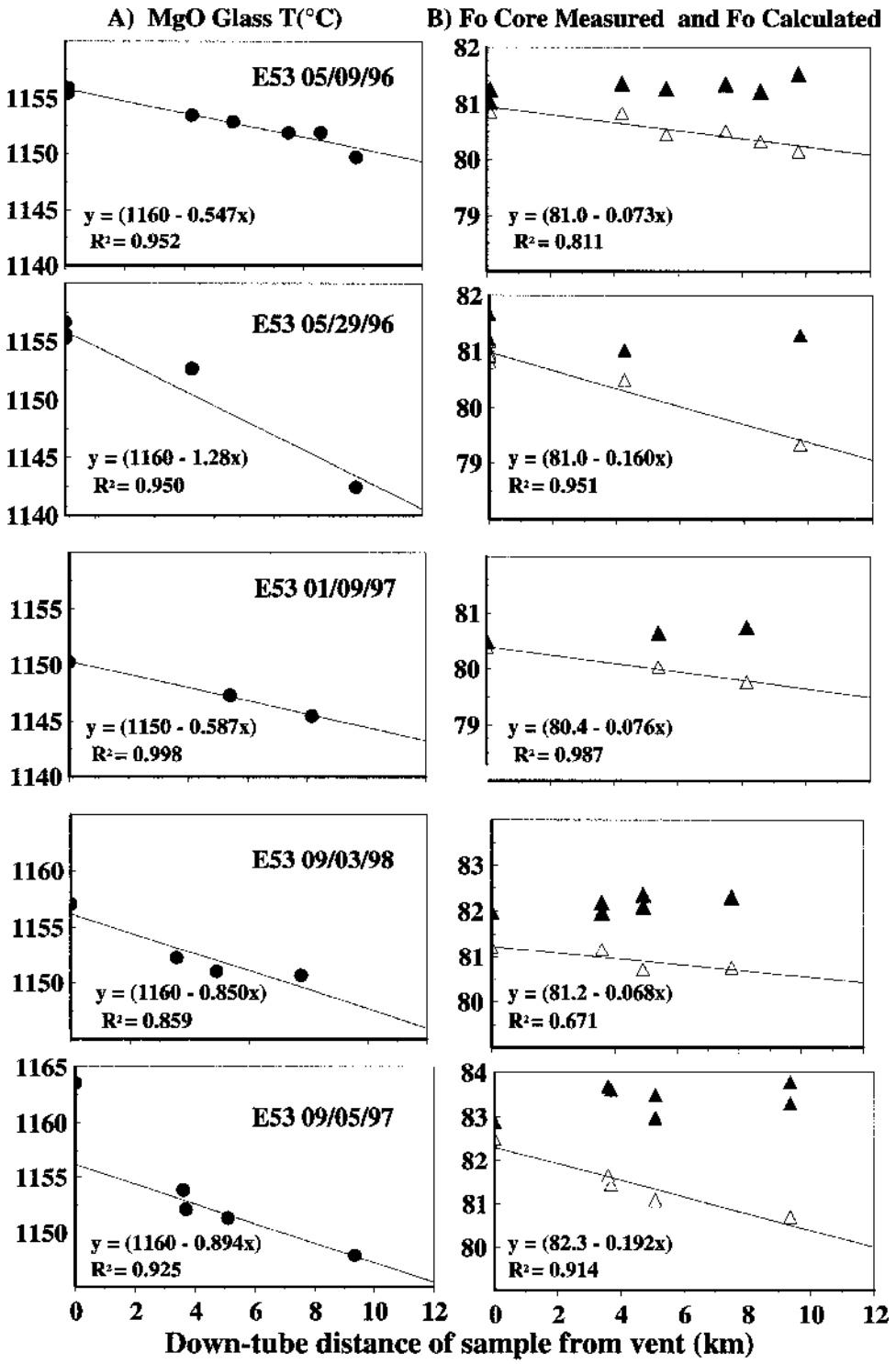
A) MgO Glass T(°C)
B) Fo Core Measured and Fo Calculated
E53 05/09/96
y = (1160 - 0.547x)
R² = 0.952
y = (81.0 - 0.073x)
R² = 0.811
E53 05/29/96
y = (1160 - 1.28x)
R² = 0.950
y = (81.0 - 0.160x)
R² = 0.951
E53 01/09/97
y = (1150 - 0.587x)
R² = 0.998
y = (80.4 - 0.076x)
R² = 0.987
E53 09/03/98
y = (1160 - 0.850x)
R² = 0.859
y = (81.2 - 0.068x)
R² = 0.671
E53 09/05/97
y = (1160 - 0.894x)
R² = 0.925
y = (82.3 - 0.192x)
R² = 0.914
Down-tube distance of sample from vent (km)

dent upon tube-transport distance. The average vent-corrected glass-temperature (T_{MgO}^*) of Episode 53 tube samples is 1154 °C (σ = 3.0) and compares to an average temperature of 1153°C for tear glasses (Appendix 1A). The vent-corrected FeO–MgO distribution coefficient (K_D^*) for type-A olivine – glass pairs in Episode 53 tube samples averages 0.295 and matches the 0.294 average of measured type-A olivine – glass K_D for tear samples during the same interval (Appendix 1A). Application of the average 0.9°C/km tube-cooling factor to late Episode 55 tube samples yields an average vent-corrected glass-temperature of 1158°C (σ = 4.0°) for this interval, which is 5°C lower than the 1163°C average for Pu‘u ‘Ō‘ō tear glasses. As discussed above, this disparity is likely due to rapid crystallization of olivine prior to cotectic crystallization of microlites below 1160°C. The vent-corrected olivine–liquid distribution coefficient is only nominally affected by the disparity in up-tube projection of glass compositions for this interval. The average K_D^* for type-A olivine in Episode 55 tube samples, 0.281, compares well with the average K_D for type-A olivine–glass in tears, 0.283 (Appendix 1D).

K_D^* values for type-B and type-C olivine core and glass pairs are similarly vent-corrected for tube samples collected during Episode 53 and 55 steady-state activity (Appendix 1). Vent-corrected data for all olivine variants in tube samples are combined with similar data on juvenile vent samples to provide a more comprehensive assessment of pre-eruptive magmatic history.

Cognate Origins of Compatible and Incompatible Olivine

Figure 13A displays the temporal variation of measured vent and vent-corrected FeO–MgO olivine–liquid distribution coefficients of type-A, -B and -C olivine in each eruptive phase. The average K_D and K_D^* determined for 312 type-A olivine – glass pairs in 221 samples is 0.288 (σ = 0.01), which is close to the experimentally determined equilibrium K_D of 0.30 (σ = 0.03) of Roeder (1974). Grains of type-A olivine, which comprise the vast majority of those analyzed, are compatible with host glasses and interpreted to have grown in host melts under near-equilibrium conditions. Values for K_D and K_D^* for type-B olivine vary from 0.145 to 0.273. These rare, low-K_D phenocrysts are not compatible with host melts, but apparently crystallized from melts that were hotter and relatively Mg-rich compared to those represented by host glasses. Type-C olivine has values of K_D and K_D^* that range from 0.318 to 0.436 and also are incompatible with host glasses, suggesting crystallization from Mg-poor, low-temperature melts.

The temporal variation in Fo contents of type-A, -B and -C olivine is compared with olivine calculated from host glasses and whole-rock compositions in Figure 13B. The averages of measured and calculated compositions of olivine for each eruptive interval are presented in Appendix 1. As follows from the near-equilibrium K_D and K_D^* values for type-A olivine – glass pairs, measured Fo contents are only slightly higher than calculated values, and both measured and calculated values vary sympathetically over time for this entire eruptive interval. The range of forsterite content of type-B olivine is higher than that calculated from host glasses, but broadly compatible with the range of Fo values calculated for bulk-rock compositions during steady eruptive intervals. This compatibility suggests that type-B crystals could have formed in melts equivalent to the bulk-rock compositions. Grains of type-C olivine have incompatibly low-Fo core compositions compared to equilibrium Fo values in their Episode 55 host-glasses.

Plots of the relation between measured and calculated compositions of olivine and between K_D and measured Fo content (Figs. 14A, B) delineate the sources of incompatible olivine crystals to be completely consanguineous with the range of magma compositions erupted during this interval, and provide additional evidence for magma mixing during and after Episode 54. For Episode 54 lava, both the most differentiated (Fissure F) and intermediate (Fissures A–E) lavas contain Fo-rich type-B olivine that is compatible with whole-rock compositions erupted during steady-state eruptive intervals. These crystals of olivine were probably mixed with magma from the steady-state rift conduit (see below). Fissure F also includes relatively low-Fo type-B olivine, similar in composition to type-A (near-equilibrium) olivine in magmas of Fissures A–E. Thus during the Episode 54 event, the most fractionated magma (Fissure F) was also mixed with melts of intermediate composition (Fissures A–E). Type-C olivine only occurs in post-Episode 54 lava. These compositions correspond to the range of type-A olivine in Episode 54 lavas and are interpreted to have been mixed into Episode 55 lava as fractionated and hybrid Episode 54 melts were flushed through the eruption conduit. The genetic association of each identified type of olivine with specific magmatic components erupted throughout this interval

FIG. 12. Compositional variations in glass and olivine *versus* distance of samples down-tube from the vent (kilometers) collected during same-day sampling experiments. The horizontal scale (distance) is the same for each figure, and linear regression for distance-variation fit is shown in each diagram. Series A (1–7): Variation in MgO-based glass temperature with down-tube distance for each of the seven same-day experiments (indicated by episode number and date in each figure). Series B (1–7): fairly constant compositions of measured type-A olivine cores (in terms of % Fo; filled triangles) are compared to olivine compositions calculated from host glasses (assuming K_D = 0.30) (open triangles) with down-tube distance.

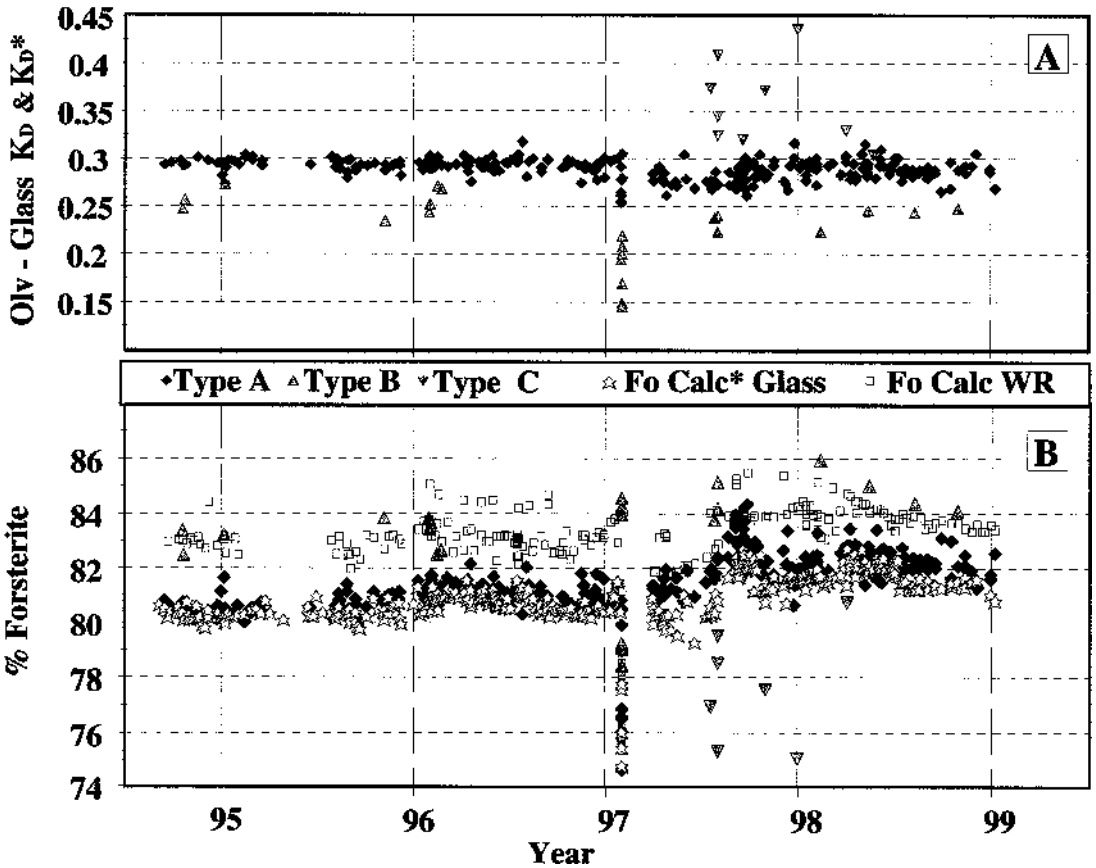

FIG. 13. Time-series plots of vent and "vent-corrected" (see text) olivine–liquid relations for samples collected from September, 1994 through December, 1998. A) Variation of K_D and K_D^* of type-A, type-B and type-C olivine (symbols shown in legend are the same as in Fig. 5C). B) Variation in % Fo of measured core compositions for type-A, type-B and type-C olivine (symbols same as in A), compared with % Forsterite calculated for whole rocks (open squares) and for vent and "vent-corrected" glasses (open stars). Calculated compositions of olivine for whole rocks, tears and vent glasses assume an equilibrium K_D of 0.300, and a vent-corrected equilibrium K_D^* is used for tube glasses (assuming a 0.002/km addition to the calculated host-glass equilibrium composition).

implies that all olivine variants have crystallized within the active shallow magmatic plumbing system. This conclusion is supported by the compatible range of compositions observed for glass inclusions in olivine (see Fig. 11).

Despite being incompatible with host glasses, the cognate association of type-B olivine within the shallow magmatic plumbing system is indicated by compatibility with the range of bulk-rock compositions erupted during steady-state activity. There are a number of good reasons for treating steady-state whole-rock compositions as representative of bulk liquids, from which type-B olivine crystallized. Whole-rock variations with time are mirrored by variations in both glasses and near-equilibrated olivine (Fig. 5), suggesting that bulk lava is not affected by either assimilation or fractionation of significantly varying amounts of olivine. As shown in Figure 15A, the bulk-rock variation in Mg with time is matched by the addition of 4% of type-A olivine to their respective host-glasses, indicating that these magmas have experienced only a small degree of near-equilibrium crystallization during pre-eruptive transit within the rift zone. Averages of olivine compositions calculated for bulk-rock liquids in Episode 53 and late Episode 55 match the average of measured type-B olivine cores for each interval, Fo_{83} and Fo_{84}, respectively (Appendix 1). Finally, the application of glass thermometry to bulk-rock compositions implies an average 30°C differential between erupted glasses and bulk liquids for Episode 53 and Episode 55 lavas (Fig. 15B, Appen-

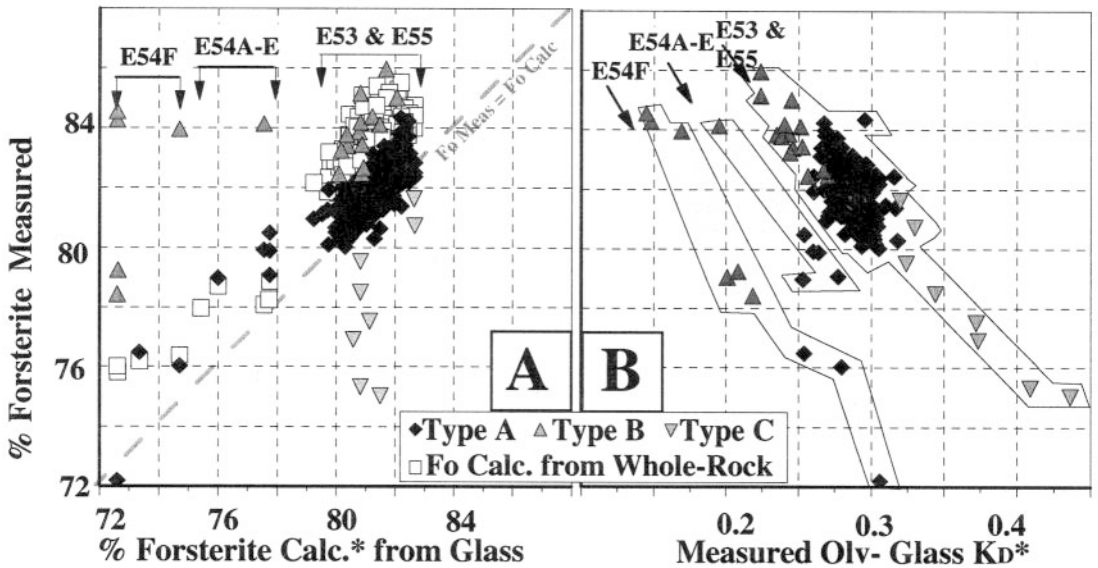

FIG. 14. Measured composition (% Fo) of type-A, type-B and type-C olivine cores plotted (symbols same as in Fig. 15) *versus* calculated olivine–liquid parameters delineate sources of incompatible olivine in each eruptive group. A) Olivine core compositions are plotted along with calculated % Forsterite for whole-rock compositions (assuming $K_D = 0.30$) (open squares) *versus* % Forsterite calculated for host glasses (using $K_D^* = 0.002/\text{km} + 0.300$; see explanation in text). B) Olivine-core compositions *versus* K_D^* measured for coexisting olivine and host glasses. Samples from different eruptive intervals (Episodes 53–55 and Episode 54, Fissures A–E and F) are distinguished in each diagram.

dix 1). This difference in temperature corresponds to an independently determined 30°C difference interpolated from the Roeder–Emslie olivine saturation-surface using averaged type-A olivine – glass and type-B olivine – bulk-rock pairs (see Fig. 7 of Roeder & Emslie 1970).

DISCUSSION

Olivine–liquid relations, if correlated in time and space with the physical behavior of Kīlauea volcano from 1994 through 1998, reveal key aspects of magma transport and storage within the shallow plumbing system that feeds the ongoing rift-zone eruption. Kīlauea's active summit-to-rift-zone magma conduit was initially established by down-rift dike propagation from the summit region at the onset of this eruption in 1983 (Okamura *et al.* 1988). Subsequent near-continuous transport of magma through this conduit has produced a well-worn, 16-km-long pipeline between the summit magma chamber and the Pu'u 'Ō'ō vent. The maintenance of an efficient hydrostatic balance within this shallow magmatic plumbing system is indicated by deformational signatures at the summit that precede short-term fluctuations in eruptive vigor during periods of steady-state activity (Thornber *et al.* 1995, 1996). Continuous GPS (Global Positioning System) measurements from June 1996 through December 1998 indicate summit extension and contraction (inflation and deflation) and broadly correlate with temperature and compositional variations of eruptive products along the east rift-zone for this interval (Fig. 15A). In general, erupted magmas become hotter and more Mg-rich in response to summit inflation, and cooler and poorer in Mg when the summit deflates. Sudden and rapid inflation of the summit may result from either convective overturn of the subcaldera magma chamber (associated with degassing and rapid expansion in volume) or from the injection of new magma into the system. Such events are typically succeeded by a period of steady deflation until steady-state hydrostatic pressure is re-established within the summit-rift zone conduit. Sudden and rapid deflation of the summit occurs in response to diversion of magma from the summit chamber associated with shallow rift-zone extension and intrusion events. The Nāpau Crater eruption in January 1997 was such an event, and was succeeded by gradual inflation of the summit until steady-state activity was re-established at Pu'u 'Ō'ō.

Considering the correlation between eruptive compositions and magmatic pressure within the continually recharged summit-rift zone plumbing system, it is reasonable to infer that uniform bulk-liquid temperatures during prolonged steady-state activity (averaging 1184° to 1194°C in Episodes 53 and 55, Appendix 1) represent temperatures of magma in the shallow summit re-

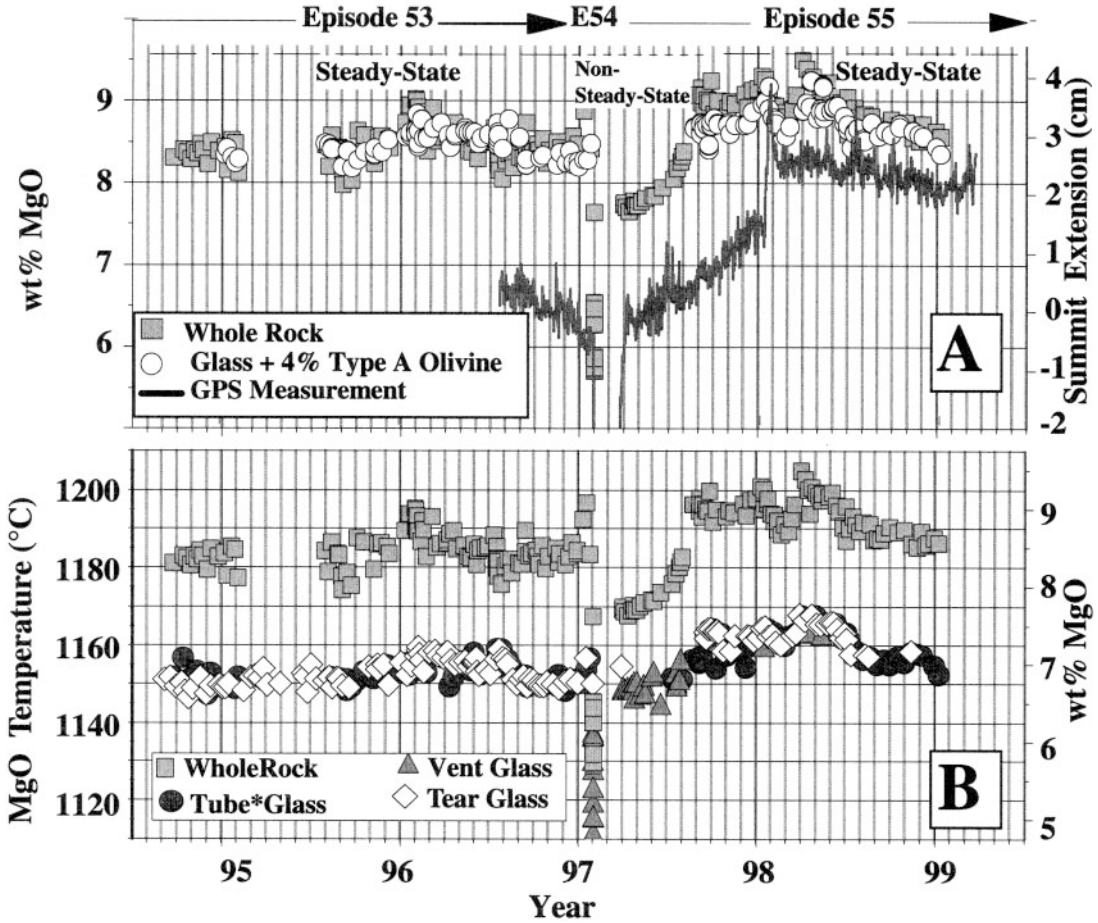

FIG. 15. Time-series plots for samples collected from September, 1994 through December, 1998. A) MgO-based temperature and wt% MgO for tear, vent and distance-corrected tube glasses (symbols same as those in Fig. 5 for tear, tube and vent samples) and for bulk lava samples (shaded squares). B) Host-glass composition adjusted for additional 4% of coexisting type-A olivine (open diamonds) are compared with bulk-lava compositions. Continuous GPS measurement of horizontal extension of the summit relative to the southern flank of Kīlauea is shown as a solid line (plotted as centimeters against the right Y-axis).

gion. Thus the near-equilibrium relation of type-B olivine with bulk liquids suggests that these crystals of olivine grew within the summit magma chamber and were subsequently included in the rift-zone conduit. Theoretical and experimental work of Donaldson (1975, 1976) demonstrates that unzoned grains of equilibrium olivine, with morphological development similar to that of type-A olivine in steady-state lava, grow at rates between 2.1 and 6.1 $\times$ 10^{-7} cm s^{-1} at 10–30°C of undercooling. If similar parameters apply to near-equilibrium type-A olivine in the steady-state pre-eruptive regime, it follows that these crystals of olivine may have grown during the 30°C of cooling associated with magma transport along the summit – rift-zone conduit. Accordingly, an estimate of both transport and cooling rates along the summit – rift-zone conduit may be made from calculations of olivine growth-rate. If olivine nucleated heterogeneously around grains of chromian spinel (commonly included by type-A olivine) or around pre-existing nuclei of olivine, it is possible that type-A olivine began to grow under conditions at or near the summit reservoir. With an approximate growth-rate of 5 $\times$ 10^{-7} cm s^{-1}, the average 0.07 cm crystal of type-A olivine would grow in approximately 38 hours. An average ΔT between summit-derived bulk liquids and erupted lava of 30°C implies an average cooling rate of ~2°C/hour along the 16-km rift-zone conduit, which is slow enough to maintain near-equilibrium growth of olivine (G.

Lofgren, pers. commun., 1999). This calculation of olivine growth-rate also implies that magma is moving at ~2 km/hr through the conduit. The preponderance of a subhedral morphology of these phenocrysts is consistent with mechanical erosion associated with dynamic growth and transport in such an environment. An additional measure of support for the summit – rift-zone conduit origin of type-B and type-A olivines is the relatively high sulfur content of their glass inclusions, which suggests crystallization in such undegassed pre-eruptive environments. Although not quantified by detailed diffusion profiles, the development of more extensive rims in type-B olivine (Fig. 8) is consistent with intracrystalline diffusion produced during rift-conduit transport, as calculated using parameters and equations of Buening & Buseck (1973). A first-order calculation suggests a maximum rim development of ~0.02 mm in 40 hours, assuming that cooling with transport is approximated by an average diffusion-coefficient of 2.67×10^{-11} cm s^{-1} between Fo_{84} olivine and a melt in equilibrium with Fo_{80} olivine.

The January 30, 1997 (Episode 54) event was immediately preceded by sudden shallow east-rift extension (<2.3 km beneath the vicinity of Nāpau Crater). The sudden offset of the hydrostatic balance in the active summit – rift-zone conduit system is reflected by the radical deflation of the summit associated with this event (Fig. 15A). Modeling of continuous GPS data encompassing the summit and upper east rift-zone areas for this interval (Owen *et al.* 1997) indicates that the sudden extension within the eruptive plumbing system allowed the influx and mixing of magma derived from beneath the summit, from the upper rift-zone and from beneath Pu‘u ‘Ō‘ō. The range of relative low-temperature, fractionated lava compositions erupted during Episode 54 (Figs. 5, 6) is likely to have been produced by a mixture of Episode 53 eruption-conduit magmas and rift-stored magmas that were emplaced beneath Nāpau crater during the early phases of this eruption in 1983. Details of major-element, trace-element and volume models quantifying this process are beyond the scope of the present study. However, as outlined above, the crystals of incompatible olivine present in both intermediate and more fractionated Episode 54 magmas have a compositional fingerprint of type-A and type-B olivines of summit – rift-zone conduit magmas and thus identifies their presence as a mixing component.

In early 1997, before Episode 55 steady-state eruptive conditions were re-established, there was a steady increase of lava temperature and whole-rock wt% MgO associated with gradual inflation of the summit (Fig. 15A). Lava issued from sporadically active Pu‘u ‘Ō‘ō flank vents during this interval contains a myriad of incompatible olivine phenocrysts (Figs. 4, 5C and 13) reflecting a complex mixture of entrained hybrid components. Crystals of type-C olivine with reverse zoning have Mg-poor core fingerprints that identify them as having initially grown in the hybrid fractionates of Episode 54 magmas. Some crystals of type-C olivine display complex core–rim relations reflecting a diverse Mg-poor, Mg-rich and host-equilibrated compositional history, whereas others have included plagioclase crystallized at temperatures lower than the host olivine. There are also remnants of reacted Mg-rich, summit-derived type-B olivine that must have resided in lower-temperature rift magmas. These incompatible olivine – liquid relations apply primarily to the post-episode 54 interval, during which the summit – rift-zone eruptive conduit was undergoing magmatic re-pressurization. Combined petrological and geodetic evidence suggests a temperature–composition history related to gradual flushing of rift-stored components introduced into the active rift-zone conduit as a result of the Episode 54 extensional event.

During steady-state activity of later Episode 55, the hottest lavas of this entire eruption contained the most magnesian type-A olivine found to date. This finding may be explained by a combination of factors involving 1) replenishment of the post-Episode 54 deflated summit reservoir with hotter magma, and 2) development of a more efficient configuration of the conduit as a result of shallow extension along the rift zone during Episode 54.

Conclusions

Olivine–liquid relations of lava erupted by Kīlauea Volcano from 1994 to 1998 provide a petrological record of summit – rift-zone conduit characteristics during intervals of both steady-state and non-steady-state activity. During intervals of continuous eruption, the composition of vent lava and tube lava (corrected to vent conditions) is restricted to a narrow range governed by equilibrium crystallization of olivine during shallow pre-eruptive storage and transport of magma. These subtle changes in lava composition are influenced by changes in magmatic pressure that originate beneath the summit and are transmitted through a hydrostatically balanced summit – rift-zone plumbing system. The artesian-like behavior of this plumbing system suggests that the long-lived Pu‘u ‘Ō‘ō eruption is fed by a dynamically replenished magmatic “aquifer” that extends 16 km down-rift from the summit magma chamber. The efficiency of magma transport within the molten “aquifer” is unknown, but results of this study suggest that mass transfer may occur within 2 days or less.

Dynamic processes associated with episodic flushing of stagnant rift-zone pockets of magma are documented in this eruptive interval. In January 1997, long-term steady-state magmatic effusion through the rift-zone conduit was disrupted by an abrupt release of confining pressure associated with a shallow extensional event beneath Nāpau Crater. Eruptive fissures issued distinct compositions of lava and phenocrysts derived from mixtures of cooler magma, stored beneath Nāpau Crater, with hotter, summit-derived components. Sub-

sequent to the Nāpau Crater event, progressive removal of this rift-stored magma component is documented by a temporal decrease in hybrid olivine–liquid relations. The gradual change to uncontaminated compositions derived from the summit magma chamber is linked temporally to summit inflation and associated with re-pressurization of the magmatic "aquifer" by a steady influx of new magma.

Renewed steady-state activity at Pu'u 'Ō'ō was characterized by continuous effusion of the most primitive olivine-controlled magmas observed thus far in this eruption, suggesting efficient transport of summit-derived magma to the east-rift-zone eruption. The shallow magmatic plumbing system associated with this epoch of shield-building activity at Kīlauea Volcano continues to be hydraulically driven by a seemingly endless supply of olivine-saturated magma. Barring any structural displacements within the summit – rift-zone conduit that would affect diversion of magma transport through the east-rift-zone, it appears likely that the 18-year-old and ongoing eruption of Kīlauea will continue into the foreseeable future.

Acknowledgements

This paper was improved by formal reviews from Kathy Cashman, Roz Helz and Bob Tilling. Ken Hon, Dave Clague and Peter Roeder contributed thoughts and discussion to this effort. Greg Meeker (USGS Denver Microbeam Facility) is gratefully acknowledged for sharing his scientific and technical expertise and providing assistance with electron-microprobe analyses and for the scanning electron imagery used in this investigation. Dave Seims (USGS Denver XRF facilities) completed all major-element analyses with incredible efficiency. Geological sampling for this investigation was conducted as part of routine eruption monitoring conducted by the USGS Hawaiian Volcano Observatory. Colleagues at HVO who contributed to the mapping and sampling that are reported in this paper include: C. Heliker, J. Kauahikaua, D. Sherrod, T. Mattox, F. Trusdell, L. Kezsthelyi and M. Mangan. Also, the continuous GPS data for Kīlauea was provided by M. Lisowski, A. Miklius and M. Sako (HVO, USGS). Numerous HVO "Geology Group volunteers" provided sample preparation and data archiving. I especially thank Doug Goehring, Mike Cazeneuve, Kate Kenedy, Nadine Calas, Sarah Hoover, Emily Hunt, Chris Eisinger, and Chris Surmonte for their outstanding support in this regard. This manuscript is dedicated to my former advisor, Prof. Peter L. Roeder.

References

Buening, D.K. & Buseck, P.R. (1973): Fe–Mg lattice diffusion in olivine. *J. Geophys. Res.* **78**, 6852-6862.

Cashman, K.V., Mangan, M.T. & Newman, S. (1994): Surface degassing and modifications to vesicle size distributions in active basalt flows. *J. Volcanol. Geotherm. Res.* **61**, 45-68.

_____, Thornber, C.R. & Kauahikaua, J.P. (1999): Cooling and crystallization of lava in open channels, and the transition of pahoehoe lava to 'a'a, 1999. *Bull. Volcanol.* **61**, 306-323.

Clague, D.A., Moore, J.G., Dixon, J.E. & Friesen, W.B. (1995): Petrology of submarine lavas from Kilauea's Puna Ridge, Hawaii. *J. Petrol.* **36**, 299-349.

Donaldson, C.H. (1975): Calculated diffusion coefficients and the growth rate of olivine in a basalt magma. *Lithos* **8**, 163-174.

_____ (1976): An experimental investigation of olivine morphology. *Contrib. Mineral. Petrol.* **57**, 187-213.

Duffield, W.A., Gibson, E.K., Jr. & Heiken, G.H. (1977): Some characteristics of Pele's hair. *J. Res. U.S. Geol. Surv.* **5**, 93-101.

Garcia, M.O., Ho, R.A., Rhodes, J.M. & Wolfe, E.W. (1989): Petrologic constraints on rift-zone processes: results from episode 1 of the Puu Oo eruption of Kilauea volcano, Hawaii. *Bull. Volcanol.* **52**, 81-96.

_____, Rhodes, J.M., Trusdell, F.A. & Pietruszka, A.J. (1996): Petrology of lavas from the Puu Oo eruption of Kilauea Volcano. III. The Kupaianaha episode (1986–1992). *Bull. Volcanol.* **58**, 359-379.

_____, _____, Wolfe, E.W., Ulrich, G.E. & Ho, R.A. (1992): Petrology of lavas from episodes 2–47 of the Puu Oo eruption of Kilauea Volcano, Hawaii: evaluation of magmatic processes. *Bull. Volcanol.* **55**, 1-16.

Harris, A.J.L. & Thornber, C.R. (1999): Complex effusive events at Kīlauea as documented by the GOES satellite and remote video cameras. *Bull. Volcanol.* **61**, 382-395.

_____, _____, Kauahikaua, J., Sherrod, D., Trusdell, F., Sawyer, M.W., Flament, P., Keszthelyi, L., Flynn, L.P. & Mouginis-Mark, P.J. (1998): Chronology of the episode 54 eruption at Kilauea Volcano, Hawaii, from GOES–9 satellite data. *Geophys. Res. Lett.* **24**, 3281-3284.

Heliker, C.C., Mangan, M.T., Mattox, T.N., Kauahikaua, J.P. & Helz, R.T. (1998): The character of long-term eruptions: inferences from episodes 50–53 of the Pu'u 'Ō'ō – Kupaianaha eruption of Kilauea Volcano. *Bull. Volcanol.* **59**, 381-393.

_____, Ulrich, G.E., Margriter, S.C. & Hoffmann, J.P. (2000): Maps showing the development of the Pu'u 'Ō'ō – Kupaianaha flow field, June 1984 – February 1987, Kīlauea Volcano, Hawai'i. *U.S.Geol. Surv., Misc. Invest. Ser., Map* **I-2685** (four sheets).

HELZ, R.T. (1987): Diverse olivine types in lava of the 1959 eruption of Kilauea volcano and their bearing on eruption dynamics. *U.S. Geol. Surv., Prof. Pap.* **1350**, 691-722.

_____, BANKS, N.G., HELIKER, C., NEAL, C.A. & WOLFE, E.W. (1995): Comparative geothermometry of recent Hawaiian eruptions. *J. Geophys. Res.* **100**, 17,637-17,657.

_____ & HEARN, B.C., JR. (1998): Compositions of glasses from the Pu'u 'Ō'ō – Kupaianaha eruption of Kilauea Volcano, Hawaii: January 1983 through December 1994. *U.S. Geol. Surv., Open File Rep.* **98-511**.

_____, HELIKER, C.C., MANGAN, M.T., HON, K., NEAL, C.A. & SIMMONS, L. (1991): Thermal history of current Kilauean East Rift eruption. *Trans. Am. Geophys. Union* (*Eos*) **72**, 557-558 (abstr.).

_____, HON, K. & HELIKER, C. (1993): Thermal efficiency of lava tubes at Kilauea Volcano, Hawaii. *Int. Assoc. Volcanol. Chem. Earth's Interior, Abstr.* (*Canberra*), 47.

_____ & THORNBER, C.R. (1987): Geothermometry of Kilauea Iki lava lake, Hawaii. *Bull. Volcanol.* **49**, 651-668.

_____ & WRIGHT, T.L. (1992): Differentiation and magma mixing on Kilauea's East Rift Zone. A further look at the eruptions of 1955 and 1960. 1. The late 1955 lavas. *Bull. Volcanol.* **54**, 361-384.

HUEBNER, J.S. & WOODRUFF, M.E. (1985): Compositions and critical evaluation of microprobe standards available in the Reston microprobe facility. *U.S. Geol. Surv., Open File Rep.* **85-718**.

JAROSEWICH, E., NELEN, J.A. & NORBERG, J.A. (1979): Electron microprobe reference samples for mineral analysis. *Smithsonian Contrib. Earth Sci.* **22**, 68-72.

KAUAHIKAUA, J.P., CASHMAN, K.V., MATTOX, T.N., HELIKER, C.C., HON, K.A., MANGAN, M.T. & THORNBER C.R. (1998): Observations on basaltic lava streams in tubes from Kīlauea Volcano, island of Hawai'i. *J. Geophys. Res.* **103**, 27,303-27,323.

_____, MANGAN, M.T., HELIKER, C.C. & MATTOX, T.N. (1996): A quantitative look at the demise of a basaltic vent: the death of Kupaianaha, Kilauea Volcano, Hawai'i. *Bull. Volcanol.* **57**, 641-648.

KESZTHELYI, L. (1995): A preliminary thermal budget for lava tubes on the Earth and planets. *J. Geophys. Res.* **100**, 20,411-20,420.

MANGAN, M.T., HELIKER, C.C., MATTOX, T.N., KAUAHIKAUA, J.P. & HELZ, R.T. (1995): Episode 49 of the Pu'u 'Ō'ō – Kupaianaha eruption of Kilauea Volcano – breakdown of a steady-state eruptive era. *Bull. Volcanol.* **57**, 127-135.

MATTOX, T.N., HELIKER, C., KAUAHIKAUA, J. & HON, K. (1993): Development of the 1990 Kalapana Flow Field, Kilauea Volcano, Hawai'i. *Bull. Volcanol.* **55**, 407-413.

OKAMURA, A.T., DVORAK, J.J., KOYANAGI, R.Y. & TANAGAWA, W.R. (1988): Surface deformation during dike propagation. *U.S. Geol. Surv., Prof. Pap.* **1463**, 165-181.

OWEN, S., SEGALL, P., LISOWSKI, M., MIKLIUS, A., BEVIS, M. & FOSTER, J. (1997): The January 30, 1997 fissure eruption in Kilauea's east rift zone as measured by continuous GPS. *Trans. Am. Geophys. Union* (*Eos*) **78**, S105 (abstr.).

ROEDER, P.L. (1974): Activity of iron and olivine solubility in basaltic liquids. *Earth Planet. Sci. Lett.* **3**, 397-410.

_____ & EMSLIE, R.F. (1970): Olivine–liquid equilibrium. *Contrib. Mineral. Petrol.* **29**, 275-289.

SAKIMOTO, S.E.H., CRISP, J. & BALOGA, S.M. (1997): Eruption constraints on tube-fed planetary lava flow. *J. Geophys. Res.* **102**, 6597-6613.

SCHWINDINGER, K.R. & ANDERSON, A.T., JR. (1989): Synneusis of Kilauea Iki olivines. *Contrib. Mineral. Petrol.* **103**, 187-198.

SHARMA, K., SELF, S., THORNBER, C.R., KESZTHELYI, L. & THORDARSON, T. (1999): Textural variations through inflated pahoehoe flow lobes from Kilauea, Hawaii. *Trans. Am. Geophys. Union* (*Eos*) **80**, 46 (abstr.).

SHIMOZURU, D. (1994): Physical parameters governing the formation of Pele's hair and tears. *Bull. Volcanol.* **56**, 217-219.

SWANSON, D. (1973): Pahoehoe flows from the 1969–1971 Mauna Ulu eruption, Kīlauea Volcano, Hawaii. *Geol. Soc. Am., Bull.* **84**, 615-626.

TAGGART, J.E., JR., LINDSAY, J.R., SCOTT, B.A., VIVIT, D.V., BARTEL, A.J. & STEWART, K.C. (1987): Analysis of geological materials by wavelength-dispersive X-ray fluorescence spectrometry. *In* Methods for Geochemical Analysis (P.H. Baedecker, ed.). *U.S. Geol. Surv., Bull.* **1170**, E1-E19.

THOMPSON, R.N. & TILLEY, C.E. (1969): Melting and crystallization relations of Kilauean basalts of Hawaii. The lavas of the 1959–60 Kilauea eruption. *Earth Planet. Sci. Lett.* **5**, 469-477.

THORNBER, C.R., HELIKER, C.C., REYNOLDS, J.R., KAUAHIKAUA, J.P., OKUBO, P., LISOWSKI, M., SUTTON, J. & CLAGUE, D. (1996): The eruptive surge of February 1, 1996: a highlight of Kilauea's ongoing East Rift Zone eruption. *Trans. Am. Geophys. Union* (*Eos*) **77**, 798 (abstr.).

_____ & HUEBNER, J.S. (1985): Dissolution of olivine in basaltic liquids: experimental observations and applications. *Am. Mineral.* **70**, 934-945.

_____, MATTOX, T.N., SUTTON, A.J., ELIAS,T., OKUBO, P., TOMORI, A.H. & DENLINGER, R.P. (1995): The eruptive pulse of Kilauea Volcano as revealed by continuous temperature monitoring of an active lava tube. *Trans. Am. Geophys. Union* (*Eos*) **76**, 681 (abstr.).

_____, ROEDER, P.L. & FOSTER, J.R. (1980): The effect of composition on ferric-ferrous ratio in basaltic liquids at atmospheric pressure. *Geochim. Cosmochim. Acta* **44**, 525-532.

_____, SHERROD, D., HELIKER, C.C., KAUAHIKAUA, J.P., TRUSDELL, F., LISOWSKI, M. & OKUBO, P. (1997): Kilauea's on going eruption: Nāpau Crater revisited after 14 years. *Trans. Am. Geophys. Union* (*Eos*) **78**, S329 (abstr.).

TILLING, R.I. & DVORAK, J.J. (1993): Anatomy of a basaltic shield volcano. *Nature* **363**, 125-133.

WOLFE, E.W., NEAL, C.A., BANKS, N.G. & DUGGAN, T.J. (1988): Geologic observations and chronology of eruptive events. *In* The Puu Oo Eruption of Kilauea Volcano, Hawaii: Episodes 1 through 20, January 3, 1983, through June 8, 1984 (E.W. Wolfe, ed.). *U.S. Geol. Surv., Prof. Pap.* **1463**, 1-97.

WRIGHT, T.L. (1971): Chemistry of Kilauea and Mauna Loa lava in space and time. *U.S. Geol. Surv., Prof. Pap.* **735**.

_____ & FISKE, R.S. (1971): Origin of the differentiated and hybrid lavas of Kilauea Volvano, Hawaii. *J. Petrol.* **12**, 1-65.

Received January 6, 2000, revised manuscript accepted August 17, 2000.

Appendix 1A - Episode 53 (Steady-State): Averaged Glass, Olivine, Inclusion and Whole-Rock Chemistry

Pu'u 'O'ō Tears - 9/06/94 to 1/29/97

Sample Numbers: KE53-1533T to -1846T

GLASS

90 samples, 10 analyses each

	Avg	StdDev	Min	Max
SiO_2	51.38	0.48	50.48	52.45
Al2O3	13.46	0.21	12.25	13.90
FeOt	10.99	0.11	10.77	11.23
MgO	6.90	0.16	6.59	7.24
CaO	10.95	0.11	10.58	11.23
Na2O	2.35	0.09	2.05	2.81
K2O	0.43	0.02	0.38	0.46
TiO2	2.42	0.06	2.28	2.55
P2O5	0.24	0.01	0.21	0.27
MnO	0.16	0.01	0.12	0.19
Total	99.27			
Sppm	bdl			336
MgO T(°C)	1153	3	1146	1160
Calc Fo	80.6	0.3	79.8	81.3
Actual Tube Distance				
Vent Corrected T(°C)				
Vent Corrected Calc FO*				

TYPE A OLIVINE CORES

60 cores in 42 samples

	Avg	StdDev	Min	Max
SiO2	39.56	0.47	38.26	40.46
FeO	17.97	0.39	16.97	18.60
MgO	42.49	0.67	40.58	43.70
CaO	0.26	0.02	0.23	0.31
MnO	0.23	0.02	0.18	0.28
NiO	0.19	0.02	0.15	0.22
Total	100.70			
% Fo	80.8	0.4	80.0	82.0
Size (mm)	0.63	0.39	0.20	2.00
Ol/Liq KD	0.294	0.006	0.272	0.305
Vent Corrected KD*				

TYPE B OLIVINE CORES

2 cores in 2 samples

	Avg	StdDev	Min	Max
	39.73	0.03	39.71	39.76
	16.12	0.33	15.79	16.44
	43.67	0.31	43.36	43.99
	0.23	0.00	0.23	0.23
	0.22	0.01	0.21	0.22
	99.96			
	82.8	0.4	82.5	83.2
	0.55	0.05	0.50	0.60
	0.250	0.006	0.244	0.257

TYPE A OLV INCLUSIONS

11 inclusions in 10 samples

	Avg	StdDev	Min	Max
SiO2	51.57	0.39	50.78	52.33
Al2O3	13.53	0.13	13.37	13.77
FeOt	11.03	0.22	10.68	11.37
MgO	6.71	0.15	6.46	6.95
CaO	10.95	0.17	10.71	11.31
Na2O	2.37	0.05	2.29	2.49
K2O	0.43	0.02	0.41	0.46
TiO2	2.43	0.06	2.34	2.54
P2O5	0.24	0.03	0.19	0.29
MnO	0.17	0.02	0.14	0.21
Total	99.43			
Sppm	353	90	168	461
MgO T(°C)	1149	3	1144	1154
Calc Fo	80.1	0.3	79.5	80.4
Olv/Inc KD	0.283	0.008	0.277	0.299

TYPE B OLV INCLUSIONS

1 inclusion in 1 sample

	Avg
	52.22
	13.73
	10.77
	6.44
	10.87
	2.33
	0.43
	2.49
	0.30
	0.24
	99.82
	437
	1143
	79.8
	0.252

WHOLE ROCK (XRF)

6 samples

	Avg	StdDev	Min	Max
SiO2	50.39	0.04	50.51	50.64
Al2O3	13.12	0.12	12.95	13.33
FeOt	11.61	0.07	11.52	11.72
MgO	8.49	0.28	7.98	8.91
CaO	10.81	0.09	10.64	10.90
Na2O	2.13	0.02	2.11	2.16
K2O	0.42	0.01	0.41	0.43
TiO2	2.42	0.03	2.37	2.46
P2O5	0.25	0.01	0.24	0.26
MnO	0.17	0.00	0.17	0.18
Total	100.00			
MgO T(°C)	1185	6	1174	1193
Calc Fo	82.8	0.5	81.8	83.5

Upper Elevation Tube Samples - 9/22/94 to 1/23/97

Sample Numbers: KE53-1536F to -1842F

GLASS

78 samples, 10 analyses each

	Avg	StdDev	Min	Max
	51.43	0.57	49.51	52.51
	13.52	0.18	12.95	14.02
	10.96	0.13	10.67	11.32
	6.76	0.15	6.51	7.10
	11.00	0.13	10.64	11.42
	2.37	0.08	2.18	2.69
	0.43	0.02	0.38	0.47
	2.44	0.07	2.30	2.64
	0.24	0.02	0.20	0.28
	0.16	0.01	0.14	0.19
	99.30			
	bdl			223
	1150	3	1145	1157
	80.3	0.4	79.2	81.1
	4.3	1.1	0.8	5.9
	1154	3	1148	1160
	80.8	0.4	79.7	81.5

TYPE A OLIVINE CORES

94 cores in 67 samples

	Avg	StdDev	Min	Max
	39.43	0.83	36.25	40.38
	17.75	0.38	16.69	18.55
	42.60	0.58	41.10	43.82
	0.27	0.02	0.23	0.47
	0.23	0.02	0.18	0.28
	0.18	0.02	0.11	0.23
	100.46			
	81.1	0.4	80.1	82.1
	0.73	0.32	0.20	2.00
	0.286	0.005	0.263	0.297
	0.295	0.006	0.275	0.309

TYPE B OLIVINE CORES

6 cores in 6 samples

	Avg	StdDev	Min	Max
	39.98	0.30	39.53	40.34
	15.94	0.45	15.41	16.63
	44.54	0.48	43.92	45.15
	0.24	0.01	0.22	0.26
	0.20	0.02	0.16	0.22
	0.24	0.03	0.21	0.30
	101.14			
	83.3	0.5	82.5	83.9
	0.60	0.10	0.05	0.70
	0.246	0.013	0.224	0.264
	0.26	0.012	0.234	0.273

TYPE A OLV INCLUSIONS

43 inclusions in 30 samples

	Avg	StdDev	Min	Max
	51.29	0.71	49.21	52.26
	13.66	0.24	13.09	14.32
	10.93	0.22	10.51	11.64
	6.49	0.35	5.30	6.89
	11.17	0.32	10.71	12.36
	2.35	0.08	2.02	2.48
	0.42	0.02	0.36	0.45
	2.43	0.06	2.29	2.56
	0.25	0.03	0.18	0.32
	0.16	0.02	0.13	0.20
	99.16			
	379	219	72	981
	1144	7	1121	1152
	79.6	1.0	76.6	80.7
	0.275	0.016	0.218	0.291

TYPE B OLV INCLUSIONS

2 inclusions in 2 samples

	Avg	StdDev	Min	Max
	51.07	0.24	50.83	51.31
	13.37	0.07	13.30	13.44
	11.09	0.02	11.07	11.11
	6.47	0.32	6.15	6.78
	10.94	0.02	10.92	10.95
	2.29	0.03	2.25	2.32
	0.42	0.00	0.41	0.42
	2.48	0.06	2.42	2.53
	0.25	0.01	0.24	0.26
	0.18	0.01	0.17	0.19
	98.53			
	290	178	112	469
	1144	6	1138	1150
	79.3	0.8	76.6	80.7
	0.246	0.034	0.212	0.279

WHOLE ROCK (XRF)

102 samples

	Avg	StdDev	Min	Max
	50.61	0.10	50.36	51.01
	13.19	0.15	12.87	13.58
	11.50	0.08	11.19	11.69
	8.47	0.24	7.64	9.09
	10.83	0.08	10.66	11.04
	2.15	0.04	2.06	2.30
	0.42	0.01	0.40	0.44
	2.40	0.03	2.32	2.47
	0.26	0.02	0.23	0.28
	0.17	0.00	0.17	0.18
	100.00			
	1184	5	1168	1192
	83.0	0.3	82.2	83.7

Appendix 1B Episode 54 (Nonsteady-State): Averaged Glass, Olivine, Inclusion and Whole-Rock Chemistry

Napau Fissure A,B,C,D,E - 1/30/97, 0200hrs to 1830hrs

Sample Numbers: KE54-1849S to -1860S

GLASS

5 samples, 10 analyses each

	Avg	StdDev	Min	Max
SiO2	51.08	0.29	50.85	51.65
Al2O3	13.24	0.26	12.90	13.65
FeOt	11.83	0.26	11.57	12.20
MgO	5.97	0.20	5.67	6.16
CaO	10.03	0.17	9.85	10.36
Na2O	2.65	0.07	2.56	2.74
K2O	0.63	0.02	0.60	0.67
TiO2	3.15	0.13	3.04	3.40
P2O5	0.34	0.01	0.32	0.36
MnO	0.17	0.01	0.15	0.18
Total	99.09			
Sppm	bdl			236
MgO T(°C)	1134	4	1128	1138
Calc Fo	76.9	1.0	75.4	77.7
Actual Tube Distance				
Vent Corrected T(°C)				
Vent Corrected Calc FO*				

TYPE A OLIVINE CORES

8 cores in 5 samples

	Avg	StdDev	Min	Max
SiO2	39.12	0.34	38.54	39.63
FeO	20.02	1.34	18.51	22.35
MgO	40.62	1.89	36.83	42.85
CaO	0.35	0.12	0.24	0.62
MnO	0.26	0.02	0.24	0.29
NiO	0.17	0.03	0.11	0.21
Total	100.54			
% Fo	78.3	1.9	74.6	80.5
Size (mm)	0.15	0.06	0.01	0.25
Ol/Liq KD	0.262	0.009	0.253	0.277
Vent Corrected KD*				

TYPE B OLIVINE CORES

1 core in 1 sample

	Avg
SiO2	39.84
FeO	15.14
MgO	45.06
CaO	0.23
MnO	0.19
NiO	0.22
Total	100.67
% Fo	84.1
Size (mm)	0.20
Ol/Liq KD	0.195

WHOLE ROCK (XRF)

13 samples

	Avg	StdDev	Min	Max
SiO2	50.92	0.06	50.82	51.04
Al2O3	13.88	0.06	13.77	13.97
FeOt	11.70	0.07	11.64	11.89
MgO	6.38	0.09	6.27	6.54
CaO	10.46	0.06	10.35	10.55
Na2O	2.52	0.02	2.48	2.53
K2O	0.60	0.01	0.57	0.61
TiO2	3.00	0.04	2.93	3.06
P2O5	0.36	0.01	0.35	0.37
MnO	0.17	0.00	0.17	0.17
Total	100			
MgO T(°C)	1142	2	1140	1145
Calc Fo	78.3	0.3	77.9	78.7

Napau Fissure F - 1/30/97, 2140hrs to 2/1/97 0030hrs

Sample Numbers: KE54-1861F to -1869S

GLASS

5 samples, 10 analyses each

	Avg	StdDev	Min	Max
SiO2	51.30	0.25	50.93	51.70
Al2O3	12.67	0.26	12.43	13.02
FeOt	12.55	0.20	12.16	12.74
MgO	5.14	0.19	4.87	5.44
CaO	9.18	0.13	9.05	9.35
Na2O	2.85	0.05	2.78	2.92
K2O	0.80	0.02	0.76	0.82
TiO2	3.84	0.18	3.51	4.04
P2O5	0.43	0.02	0.41	0.45
MnO	0.18	0.01	0.16	0.19
Total	98.93			
Sppm	bdl			136
MgO T(°C)	1117	4	1112	1123
Calc Fo	73.0	1.0	71.6	74.7

TYPE A OLIVINE CORES

3 cores in 3 samples

	Avg	StdDev	Min	Max
SiO2	38.52	0.27	38.14	38.72
FeO	22.99	1.45	21.84	25.03
MgO	38.54	1.49	36.46	39.85
CaO	0.26	0.03	0.21	0.29
MnO	0.30	0.01	0.29	0.31
NiO	0.14	0.02	0.11	0.17
Total	100.75			
% Fo	74.9	1.9	72.2	76.5
Size (mm)	1.00	0.71	0.50	2.00
Ol/Liq KD	0.280	0.021	0.254	0.306

TYPE B OLIVINE CORES

6 cores in 4 samples

	Avg	StdDev	Min	Max
SiO2	39.63	0.47	38.88	40.28
FeO	17.26	2.25	14.90	19.68
MgO	43.03	2.19	40.13	45.94
CaO	0.25	0.02	0.23	0.27
MnO	0.22	0.02	0.18	0.25
NiO	0.20	0.05	0.13	0.28
Total	100.58			
% Fo	81.6	2.7	78.4	84.6
Size (mm)	0.23	0.18	0.05	0.50
Ol/Liq KD	0.182	0.029	0.145	0.218

TYPE B OLV INCLUSIONS

2 inclusions in 2 samples

	Avg	StdDev	Min	Max
SiO2	52.44	0.52	51.91	52.96
Al2O3	14.61	0.08	14.53	14.69
FeOt	9.44	0.17	9.27	9.61
MgO	5.65	0.14	5.51	5.79
CaO	11.41	0.02	11.39	11.43
Na2O	2.49	0.13	2.36	2.61
K2O	0.44	0.00	0.44	0.44
TiO2	2.42	0.00	2.41	2.42
P2O5	0.24	0.02	0.22	0.26
MnO	0.16	0.00	0.16	0.16
Total	99.28			
Sppm	1029	8	1021	1037
MgO T(°C)	1128	3	1125	1130
Calc Fo	79.8	0.1	79.7	79.9
Olv/Inc KD	0.219	0.001	0.218	0.220

WHOLE ROCK (XRF)

9 samples

	Avg	StdDev	Min	Max
SiO2	51.20	0.05	51.12	51.29
Al2O3	13.72	0.03	13.69	13.79
FeOt	12.05	0.04	11.99	12.13
MgO	5.80	0.06	5.71	5.90
CaO	9.73	0.05	9.67	9.81
Na2O	2.72	0.02	2.69	2.76
K2O	0.71	0.01	0.68	0.73
TiO2	3.46	0.04	3.37	3.51
P2O5	0.43	0.00	0.42	0.43
MnO	0.17	0.00	0.17	0.17
Total	100			
MgO T(°C)	1131	1	1129	1133
Calc Fo	76.0	0.2	75.8	76.3

Appendix 1C Early Episode 55 (Nonsteady-State): Averaged Glass, Olivine, Inclusion and Whole-Rock Chemistry

Pu'u Ō'o Flank Vents - 3/31/97 to 7/29/97

Sample Numbers: KE55-1870S to - 1910F

GLASS

20 samples, 10 analyses each

	Avg	StdDev	Min	Max
SiO2	51.53	0.31	50.33	51.89
Al2O3	13.70	0.10	13.47	13.86
FeOt	10.99	0.17	10.64	11.33
MgO	6.76	0.12	6.52	7.09
CaO	10.66	0.17	10.34	10.99
Na2O	2.41	0.07	2.28	2.56
K2O	0.43	0.02	0.38	0.45
TiO2	2.45	0.06	2.37	2.57
P2O5	0.24	0.01	0.22	0.27
MnO	0.16	0.01	0.15	0.18
Total	99.33			
Sppm	bdl			bdl
MgO T(°C)	1150	2	1145	1156
Calc Fo	80.3	0.4	79.5	81.1
Actual Tube Distance				
Vent Corrected T(°C)				
Vent Corrected Calc FO*				

TYPE A OLIVINE CORES

20 cores in 18 samples

	Avg	StdDev	Min	Max
SiO2	39.68	0.26	38.97	40.09
FeO	17.49	0.36	16.89	18.04
MgO	43.00	0.36	42.21	43.57
CaO	0.26	0.01	0.22	0.28
MnO	0.23	0.01	0.20	0.26
NiO	0.19	0.02	0.15	0.25
Total	100.84			
% Fo	81.4	0.4	80.8	82.0
Size (mm)	0.75	0.42	0.24	2.00
Ol/Liq KD	0.282	0.010	0.264	0.309
Vent Corrected KD*				

TYPE B

1 core

Avg
40.06
15.60
45.18
0.23
0.18
0.24
101.48
83.8
0.75
0.241

TYPE A OLV INCLUSION

14 inclusions in 12 samples

	Avg	StdDev	Min	Max
SiO2	51.36	0.55	49.96	52.11
Al2O3	13.88	0.20	13.55	14.27
FeOt	10.95	0.32	10.03	11.35
MgO	6.40	0.25	5.99	6.79
CaO	10.92	0.22	10.49	11.31
Na2O	2.41	0.07	2.29	2.51
K2O	0.42	0.02	0.37	0.45
TiO2	2.38	0.06	2.29	2.51
P2O5	0.26	0.04	0.22	0.39
MnO	0.16	0.02	0.12	0.20
Total	99.13			
Sppm	602	231	328	1209
MgO T(°C)	1143	5	1134	1150
Calc Fo	79.4	0.8	77.8	80.7
Olv/Inc KD	0.266	0.014	0.240	0.291

WHOLE ROCK (XRF)

18 samples

	Avg	StdDev	Min	Max
SiO2	50.84	0.06	50.74	50.94
Al2O3	13.39	0.11	13.12	13.51
FeOt	11.44	0.05	11.34	11.57
MgO	7.85	0.20	7.65	8.33
CaO	10.99	0.05	10.86	11.08
Na2O	2.20	0.04	2.15	2.27
K2O	0.41	0.01	0.39	0.42
TiO2	2.41	0.02	2.36	2.43
P2O5	0.28	0.02	0.26	0.31
MnO	0.17	0.00	0.17	0.17
Total	100			
MgO T(°C)	1171	5	1168	1180
Calc Fo	82.1	0.6	81.6	82.8

Upper Elevation Tubes Samples-7/11/1997 & 8/01/97

Sample Numbers: KE55-1901F & -1911F

GLASS

2 samples, 10 analyses each

	Avg	StdDev	Min	Max
SiO2	51.57	0.12	51.45	51.69
Al2O3	13.66	0.09	13.57	13.75
FeOt	11.06	0.11	10.95	11.16
MgO	6.70	0.04	6.66	6.75
CaO	10.69	0.28	10.41	10.97
Na2O	2.47	0.01	2.46	2.47
K2O	0.40	0.03	0.38	0.43
TiO2	2.45	0.01	2.44	2.46
P2O5	0.24	0.00	0.23	0.24
MnO	0.16	0.01	0.16	0.17
Total	99.40			
Sppm	bdl			bdl
MgO T(°C)	1149	1	1148	1150
Calc Fo	80.0	0.1	80.0	80.1
Actual Tube Distance	2.9	0.8	2.1	3.7
Vent Corrected T(°C)	1152	1	1151	1152
Vent Corrected Calc FO*	80.3	0.1	80.2	80.5

TYPE A OLIVINE CORES

3 cores in 2 samples

	Avg	StdDev	Min	Max
SiO2	39.71	0.13	39.52	39.80
FeO	17.03	0.36	16.74	17.54
MgO	43.68	0.24	43.34	43.89
CaO	0.27	0.02	0.26	0.30
MnO	0.21	0.02	0.18	0.23
NiO	0.18	0.01	0.17	0.20
Total	101.08			
% Fo	82.1	0.4	81.5	82.4
Size (mm)	0.62	0.30	0.20	0.90
Ol/Liq KD	0.263	0.006	0.258	0.272
Vent Corrected KD*	0.269	0.008	0.265	0.286

TYPE B OLIVINE CORES

2 cores in 2 samples

	Avg	StdDev	Min	Max
SiO2	40.20	0.02	40.18	40.20
FeO	14.75	0.39	14.40	15.10
MgO	45.72	0.50	45.22	46.20
CaO	0.21	0.03	0.17	0.24
MnO	0.26	0.07	0.19	0.32
NiO	0.21	0.06	0.15	0.26
Total	101.34			
% Fo	84.7	0.5	84.2	85.2
Size (mm)	0.33	0.23	0.10	0.55
Ol/Liq KD	0.218	0.008	0.210	0.226
Vent Corrected KD*	0.226	0.008	0.218	0.234

TYPE C OLIVINE CORES

3 cores in 2 samples

	Avg	StdDev	Min	Max
SiO2	38.91	0.37	38.40	39.29
FeO	20.73	1.46	19.28	22.73
MgO	40.73	1.33	38.90	42.01
CaO	0.29	0.02	0.26	0.32
MnO	0.27	0.03	0.23	0.31
NiO	0.13	0.01	0.11	0.14
Total	101.05			
% Fo	77.8	1.8	75.3	79.5
Size (mm)	0.16	0.05	0.10	0.23
Ol/Liq KD	0.345	0.036	0.310	0.395
Vent Corrected KD*	0.353	0.036	0.318	0.403

TYPE A OLV INCLUSION

1 inclusion in 1 sample

Avg
51.39
13.97
11.20
6.64
10.75
2.51
0.43
2.42
0.26
0.17
99.74
933
1147
79.7
0.267

WHOLE ROCK (XRF)

2 samples

	Avg	StdDev	Min	Max
SiO2	50.75	0.05	50.70	50.79
Al2O3	13.21	0.04	13.17	13.25
FeOt	11.49	0.02	11.47	11.52
MgO	8.22	0.17	8.05	8.39
CaO	10.90	0.04	10.86	10.94
Na2O	2.18	0.05	2.13	2.23
K2O	0.41	0.01	0.40	0.41
TiO2	2.37	0.01	2.36	2.38
P2O5	0.30	0.00	0.30	0.30
MnO	0.17	0.00	0.17	0.17
Total	100			
MgO T(°C)	1179	3	1176	1183
Calc Fo	82.5	0.3	82.2	82.8

Appendix 1D Late Episode 55 (Steady-State): Averaged Glass, Olivine, Inclusion and Whole-Rock Chemistry

	Pu'u 'Ō'ō Tears - 9/18/97 to 11/19/98				Vents - 9/18/97 to 11/19/98				Upper Elevation Tube Samples - 8/22/97 to 1/07/99			
	Sample Numbers: KE55-1921T to -2083T				KE55-1962S to -2038S				Sample Numbers: KE55-1912F to -2089F			
	GLASS				GLASS				GLASS			
	38 samples, 10 analyses each				5 samples, 10 analyses each				56 samples, 10 analyses each			
	Avg	StdDev	Min	Max	Avg	StdDev	Min	Max	Avg	StdDev	Min	Max
SiO2	51.31	0.27	50.67	51.85	51.40	0.20	51.09	51.71	51.35	0.40	0.12	52.15
Al2O3	13.41	0.10	13.10	13.53	13.43	0.09	13.32	13.56	13.54	0.16	0.09	13.80
FeOt	10.91	0.12	10.42	11.08	10.95	0.11	10.81	11.08	10.80	0.17	0.11	11.04
MgO	7.40	0.13	7.12	7.66	7.39	0.07	7.26	7.45	6.95	0.13	0.04	7.22
CaO	10.77	0.21	10.19	11.05	10.81	0.11	10.68	10.96	10.89	0.20	0.28	11.18
Na2O	2.36	0.07	2.08	2.45	2.37	0.03	2.32	2.41	2.41	0.05	0.01	2.47
K2O	0.40	0.02	0.34	0.42	0.41	0.00	0.41	0.41	0.40	0.02	0.03	0.43
TiO2	2.38	0.04	2.26	2.44	2.40	0.02	2.36	2.42	2.41	0.04	0.01	2.47
P2O5	0.23	0.01	0.20	0.25	0.23	0.01	0.22	0.25	0.23	0.01	0.00	0.26
MnO	0.16	0.01	0.15	0.18	0.17	0.01	0.15	0.18	0.16	0.01	0.01	0.18
Total	99.33				99.55				99.15			
Sppm	102	29	bdl	164	bdl			bdl	bdl			228
MgO T(°C)	1163	3	1157	1168	1163	1	1160	1164	1154	3	1148	1159
Calc Fo	81.8	0.3	81.2	82.5	81.5	0.3	81.2	82.0	80.9	0.3	80.0	81.6
Actual Tube Distance									4.5	0.6	0.8	5.1
Vent Corrected T(°C)									1158	3	1151	1163
Vent Corrected Calc FO*									81.4	0.4	80.6	82.1
	TYPE A OLIVINE CORES				TYPE B	TYPE A OLIVINE CORES				TYPE A OLIVINE CORES				TYPE B OLIVINE CORES				TYPE C OLIVINE CORES			
	34 Cores in 28 Samples				1 in 1	13cores in 4 samples				90 cores in 56 samples				3 cores in 3 samples				4 cores in 4 samples			
	Avg	StdDev	Min	Max		Avg	StdDev	Min	Max	Avg	StdDev	Min	Max	Avg	StdDev	Min	Max	Avg	StdDev	Min	Max
SiO2	39.64	0.56	36.66	40.10	39.87	39.75	0.30	39.32	40.34	39.57	0.34	38.67	40.38	40.07	0.37	39.59	40.49	39.16	0.21	38.84	39.43
FeO	16.83	0.56	15.76	18.17	14.95	16.79	0.20	16.46	17.19	16.78	0.50	15.15	17.92	14.42	0.72	13.48	15.22	19.98	2.36	17.29	23.37
MgO	44.05	0.53	42.51	45.11	45.34	44.40	0.60	43.58	45.37	44.07	0.43	43.16	45.20	45.97	0.56	45.18	46.42	41.54	1.66	39.37	43.19
CaO	0.26	0.03	0.23	0.34	0.24	0.25	0.02	0.22	0.28	0.25	0.02	0.16	0.30	0.23	0.00	0.22	0.23	0.24	0.02	0.21	0.26
MnO	0.22	0.02	0.16	0.27	0.20	0.22	0.01	0.19	0.24	0.22	0.02	0.19	0.27	0.18	0.02	0.16	0.20	0.26	0.06	0.18	0.35
NiO	0.20	0.02	0.15	0.27	0.25	0.22	0.02	0.18	0.25	0.21	0.03	0.17	0.29	0.17	0.03	0.14	0.21	0.17	0.03	0.14	0.21
Total	101.21				100.86	101.64				101.10				101.04				101.36			
% Fo	82.3	0.6	80.7	83.5	84.4	82.5	0.3	82.0	82.9	82.4	0.6	81.3	84.3	85.0	0.8	84.1	86.0	78.7	2.6	75.0	81.6
Size (mm)	0.39	0.23	0.01	0.90	0.33	0.73	0.48	0.15	2.00	0.69	0.37	0.10	2.00	0.80	0.18	0.60	1.10	0.79	0.42	0.25	1.20
Ol/Liq KD	0.289	0.009	0.266	0.317	0.239	0.283	0.006	0.277	0.294	0.271	0.010	0.235	0.291	0.223	0.014	0.204	0.239	0.356	0.052	0.304	0.435
Vent Corrected KD*										0.281	0.009	0.25	0.31	0.233	0.014	0.214	0.249	0.359	0.045	0.306	0.436
	TYPE A OLV INCLUSION				TYPE B	TYPE A OLV INCLUSION				TYPE A OLV INCLUSION				TYPE B OLV INCLUSIONS				TYPE C OLV INCLUSIONS			
	10 inclusions in 8 samples				1 in 1	4 inclusions in 4 samples				54 inclusions in 46 samples				5 inclusions in 5 samples				2 inclusions in 2 samples			
	Avg	StdDev	Min	Max		Avg	StdDev	Min	Max	Avg	StdDev	Min	Max	Avg	StdDev	Min	Max	Avg	StdDev	Min	Max
SiO2	51.45	0.34	50.95	52.13	51.08	51.38	0.66	50.39	52.04	51.30	0.53	50.13	52.28	52.31	0.74	51.14	53.39	51.89	0.06	51.83	51.95
Al2O3	13.41	0.23	13.07	13.93	13.95	13.60	0.23	13.26	13.92	13.77	0.17	13.44	14.32	14.23	0.25	13.95	14.69	13.90	0.08	13.82	13.97
FeOt	10.84	0.28	10.38	11.23	10.17	10.84	0.09	10.71	10.95	10.66	0.41	9.41	11.17	9.14	0.78	8.18	10.29	10.31	0.78	9.53	11.09
MgO	7.15	0.24	6.51	7.55	7.37	6.93	0.28	6.47	7.21	6.58	0.43	5.27	7.13	6.42	0.53	5.63	6.88	7.07	0.07	7.00	7.13
CaO	10.65	0.29	10.24	11.06	10.98	11.14	0.12	11.00	11.32	11.10	0.30	10.50	11.99	11.44	0.29	11.01	11.83	11.19	0.22	10.97	11.40
Na2O	2.43	0.08	2.26	2.53	2.50	2.32	0.08	2.20	2.42	2.41	0.07	2.25	2.66	2.49	0.03	2.46	2.54	2.42	0.04	2.38	2.46
K2O	0.39	0.02	0.35	0.43	0.40	0.41	0.01	0.40	0.42	0.40	0.03	0.32	0.44	0.39	0.02	0.37	0.42	0.42	0.03	0.39	0.46
TiO2	2.38	0.07	2.28	2.50	2.33	2.41	0.08	2.29	2.51	2.41	0.08	2.08	2.56	2.42	0.13	2.24	2.63	2.47	0.03	2.44	2.49
P2O5	0.22	0.04	0.16	0.26	0.22	0.23	0.02	0.20	0.26	0.24	0.03	0.18	0.31	0.24	0.02	0.22	0.27	0.20	0.04	0.16	0.24
MnO	0.17	0.01	0.15	0.18	0.17	0.15	0.01	0.13	0.17	0.16	0.02	0.13	0.20	0.15	0.03	0.12	0.19	0.16	0.03	0.12	0.19
Total	99.08				99.17	99.39				99.02				99.22				100.01			
Sppm	502	182	166	757	713	425	249	100	801	510	290	40	1193	809	292	509	1314	413	8	404	421
MgO T(°C)	1158	5	1145	1166	1162	1153	6	1144	1159	1146	9	1120	1157	1143	11	1127	1152	1156	1	1155	1157
Calc Fo	81.3	0.6	79.9	82.0	82.7	81.1	0.2	80.7	81.4	80.2	1.1	77.2	82.4	81.0	2.6	78.4	84.6	81.9	1.3	80.6	83.2
Olv/Inc KD	0.272	0.011	0.252	0.285	0.265	0.275	0.008	0.263	0.283	0.259	0.020	0.212	0.292	0.264	0.037	0.216	0.323	0.385	0.032	0.353	0.416
						WHOLE ROCK (XRF)				WHOLE ROCK (XRF)											
						7 samples				68 samples											
						Avg	StdDev	Min	Max	Avg	StdDev	Min	Max								
SiO2						50.53	0.07	50.44	50.64	50.52	0.13	49.98	50.77								
Al2O3						13.13	0.10	12.97	13.27	13.17	0.16	12.89	13.45								
FeOt						11.39	0.05	11.35	11.49	11.42	0.09	11.30	11.66								
MgO						9.10	0.10	8.95	9.27	8.91	0.23	8.52	9.50								
CaO						10.54	0.04	10.48	10.60	10.63	0.07	10.46	10.93								
Na2O						2.14	0.03	2.11	2.19	2.14	0.04	2.07	2.22								
K2O						0.40	0.01	0.39	0.41	0.41	0.01	0.39	0.43								
TiO2						2.31	0.02	2.29	2.34	2.34	0.03	2.28	2.39								
P2O5						0.29	0.01	0.28	0.31	0.29	0.02	0.26	0.32								
MnO						0.17	0.00	0.17	0.17	0.17	0.00	0.17	0.18								
Total						100.00	0.29	99.95	99.88	100.00	11.96	0.00	#####								
MgO T(°C)						1197	2	1194	1200	1193	5	1185	1205								
Calc Fo						84.1	0.1	83.9	84.3	83.8	0.3	83.2	84.6								